Additionally, CSCs are slow-cycling or in the dormant phase of the cell cycle. For example, CSCs of acute myeloid leukaemia (Guan *et al,* 2003) and chronic myeloid leukaemia (Holyoake *et al,* 1999) survive in the dormant G0 phase of the cell cycle. In the case of solid tumours, liver CSCs were found to be mainly in the G0/G1 phase (Haraguchi *et al,* 2010). Thus, we addressed the relevance of CD10 for the CSC phenotype. We found that the CD10-positive subpopulation formed spheres *in vitro* and tumours *in vivo* more efficiently than the CD10-negative subpopulation. These results indicate that CD10 is closely related to tumourigenicity and self-renewal ability. Thus, it seems likely that CD10 could serve as a marker of CSCs in HNSCC.

Previously, CD44 (Prince *et al,* 2007), CD133 (Chiou *et al,* 2008) and ALDH1 (Chen *et al,* 2009) have been reported as markers of CSCs in HNSCC. However, whether CD44 and ALDH1 serve as true markers remains controversial. For instance, recent studies have shown that decreased rather than increased expression of ALDH1 is linked to poor prognosis (Koukourakis *et al,* 2012), while CD44 is expressed in normal head and neck squamous epithelium at an equivalent level to that detected in HNSCC (Chen *et al,* 2011). As for therapeutic resistance, CD44 expression was downregulated in irradiated cells when compared with that of untreated cells as determined in our cell surface antigen array assay of the HNSCC cell line BICR6. Moreover, the vast majority of FaDu and Detroit562 cells were CD44-positive irrespective of cisplatin or radiation treatment. In the case of CD133, Zhang *et al,* (2010) showed that CD133-positive cells possessed resistance to paclitaxel when compared with CD133-negative cells in oral cancer cell lines, although CD133 expression was barely detectable, even after the treatment, in the cell lines used in our study. Together, these data indicate that neither CD44 nor CD133 have pivotal roles in the therapeutic resistance of these HNSCC cell lines. Although it cannot be dismissed that the relevance of CD44 and CD133 in therapeutic resistance probably depends on the kinds of cells lines and treatments administered. Thus, further study is needed to determine the relationship between CSC-related properties and therapeutic resistant in HNSCC, including investigation into the effect of combination of CD10 and these markers (CD44, CD133, ALDH1). Especially, we consider the combination of CD10 and ALDH1, because we found these interdependent expressions.

Notably, we demonstrated that the CD10-positive subpopulation of HNSCC cells showed CSC-related properties, such as chemo and radio resistance, self-renewal capacity and tumourigenicity. To gain insight into the mechanisms by which CD10 confers CSC-related properties in HNSCC, we examined the expression of *OCT3/4*, which has a critical role in the development and self-renewal of embryonic stem cells (Nichols *et al,* 1998), and is linked to oncogenic processes (Gidekel *et al,* 2003). Chen *et al,* (2010, 2011). have shown that *OCT3/4* is upregulated in HNSCC CSCs, defined by ALDH1 positive cells, and in spheroid forming HNSCC cells. We found that *OCT3/4* expression was higher in CD10-positive cells than in CD10-negative cells, but that it was decreased following knockdown of CD10. These results indicate that increased CD10 is linked to *OCT3/4* expression. Further studies are required to address the functional relevance of CD10 to *OCT3/4* in HNSCC.

In conclusion, we have established that CD10 is associated with chemo and radio resistance, and that it confers CSC-related properties in HNSCC, probably through forced overexpression of *OCT3/4*. Together these findings suggest that CD10 may serve as a target molecule in the treatment of refractory HNSCC.

ACKNOWLEDGEMENTS

We thank Miyuki Ozaki and Yuko Noguchi for their technical support. The current study was partly funded by a Core Research Grant-in-Aid for Scientific Research from the Ministry of Education, Culture, Sports, Science and Technology, Japan; a Grant-in-Aid from the Third Term Comprehensive 10-year Strategy for Cancer Control of the Ministry of Health, Labour and Welfare, Japan; and grants from the Kobayashi Cancer Research Foundation, the Princess Takamatsu Cancer Research Fund, Japan; the SENSHIN Medical Research Foundation, Japan; and the National Institute of Biomedical Innovation, Japan.

REFERENCES

Argiris A, Karamouzis MV, Raben D, Ferris RL (2008) Head and neck cancer. *Lancet* **371**(9625): 1695–1709.

Bao S, Wu Q, McLendon RE, Hao Y, Shi Q, Hjelmeland AB, Dewhirst MW, Bigner DD, Rich JN (2006) Glioma stem cells promote radioresistance by preferential activation of the DNA damage response. *Nature* **444**(7120): 756–760.

Barr MP, Gray SG, Hoffmann AC, Hilger RA, Thomale J, O'Flaherty JD, Fennell DA, Richard D, O'Leary JJ, O'Byrne KJ (2013) Generation and characterisation of cisplatin-resistant non-small cell lung cancer cell lines displaying a stem-like signature. *PloS one* **8**(1): e54193.

Buhring HJ, Battula VL, Treml S, Schewe B, Kanz L, Vogel W (2007) Novel markers for the prospective isolation of human MSC. *Ann NY Acad Sci* **1106**: 262–271.

Chen C, Wei Y, Hummel M, Hoffmann TK, Gross M, Kaufmann AM, Albers AE (2011) Evidence for epithelial-mesenchymal transition in cancer stem cells of head and neck squamous cell carcinoma. *PloS one* **6**(1): e16466.

Chen YC, Chang CJ, Hsu HS, Chen YW, Tai LK, Tseng LM, Chiou GY, Chang SC, Kao SY, Chiou SH, Lo WL (2010) Inhibition of tumorigenicity and enhancement of radiochemosensitivity in head and neck squamous cell cancer-derived ALDH1-positive cells by knockdown of Bmi-1. *Oral Oncol* **46**(3): 158–165.

Chen YC, Chen YW, Hsu HS, Tseng LM, Huang PI, Lu KH, Chen DT, Tai LK, Yung MC, Chang SC, Ku HH, Chiou SH, Lo WL (2009) Aldehyde dehydrogenase 1 is a putative marker for cancer stem cells in head and neck squamous cancer. *Biochem Biophys Res Commun* **385**(3): 307–313.

Chiou SH, Yu CC, Huang CY, Lin SC, Liu CJ, Tsai TH, Chou SH, Chien CS, Ku HH, Lo JF (2008) Positive correlations of Oct-4 and Nanog in oral cancer stem-like cells and high-grade oral squamous cell carcinoma. *Clin Cancer Res* **14**(13): 4085–4095.

Galy A, Morel F, Hill B, Chen BP (1998) Hematopoietic progenitor cells of lymphocytes and dendritic cells. *J Immunother* **21**(2): 132–141.

Gidekel S, Pizov G, Bergman Y, Pikarsky E (2003) Oct-3/4 is a dose-dependent oncogenic fate determinant. *Cancer Cell* **4**(5): 361–370.

Guan Y, Gerhard B, Hogge DE (2003) Detection, isolation, and stimulation of quiescent primitive leukemic progenitor cells from patients with acute myeloid leukemia (AML). *Blood* **101**(8): 3142–3149.

Haraguchi N, Ishii H, Mimori K, Tanaka F, Ohkuma M, Kim HM, Akita H, Takiuchi D, Hatano H, Nagano H, Barnard GF, Doki Y, Mori M (2010) CD13 is a therapeutic target in human liver cancer stem cells. *J Clin Invest* **120**(9): 3326–3339.

Holyoake T, Jiang X, Eaves C, Eaves A (1999) Isolation of a highly quiescent subpopulation of primitive leukemic cells in chronic myeloid leukemia. *Blood* **94**(6): 2056–2064.

Kish J, Drelichman A, Jacobs J, Hoschner J, Kinzie J, Loh J, Weaver A, Al-Sarraf M (1982) Clinical trial of cisplatin and 5-FU infusion as initial treatment for advanced squamous cell carcinoma of the head and neck. *Cancer Treat Rep* **66**(3): 471–474.

Koukourakis MI, Giatromanolaki A, Tsakmaki V, Danielidis V, Sivridis E (2012) Cancer stem cell phenotype relates to radio-chemotherapy outcome in locally advanced squamous cell head-neck cancer. *Br J Cancer* **106**(5): 846–853.

Li X, Lewis MT, Huang J, Gutierrez C, Osborne CK, Wu MF, Hilsenbeck SG, Pavlick A, Zhang X, Chamness GC, Wong H, Rosen J, Chang JC (2008) Intrinsic resistance of tumorigenic breast cancer cells to chemotherapy. *J Natl Cancer Inst* **100**(9): 672–679.

Lo WL, Kao SY, Chi LY, Wong YK, Chang RC (2003) Outcomes of oral squamous cell carcinoma in Taiwan after surgical therapy: factors affecting survival. *J Oral Maxillofac Surg* **61**(7): 751–758.

Maguer-Satta V, Besancon R, Bachelard-Cascales E (2011) Concise review: neutral endopeptidase (CD10): a multifaceted environment actor in stem cells, physiological mechanisms, and cancer. *Stem Cells* **29**(3): 389–396.

Nichols J, Zevnik B, Anastassiadis K, Niwa H, Klewe-Nebenius D, Chambers I, Scholer H, Smith A (1998) Formation of pluripotent stem cells in the mammalian embryo depends on the POU transcription factor Oct4. *Cell* **95**(3): 379–391.

Piattelli A, Fioroni M, Iezzi G, Perrotti V, Stellini E, Piattelli M, Rubini C (2006) CD10 expression in stromal cells of oral cavity squamous cell carcinoma: a clinic and pathologic correlation. *Oral Dis* **12**(3): 301–304.

Prince ME, Sivanandan R, Kaczorowski A, Wolf GT, Kaplan MJ, Dalerba P, Weissman IL, Clarke MF, Ailles LE (2007) Identification of a subpopulation of cells with cancer stem cell properties in head and neck squamous cell carcinoma. *Proc Natl Acad Sci USA* **104**(3): 973–978.

Roques BP, Noble F, Dauge V, Fournie-Zaluski MC, Beaumont A (1993) Neutral endopeptidase 24.11: structure, inhibition, and experimental and clinical pharmacology. *Pharmacol Rev* **45**(1): 87–146.

Sinclair WK (1968) Cyclic X-ray responses in mammalian cells *in vitro*. *Radiation research* **33**: 620–643.

Stingl J, Raouf A, Emerman JT, Eaves CJ (2005) Epithelial progenitors in the normal human mammary gland. *J Mammary Gland Biol Neoplasia* **10**(1): 49–59.

Sunday ME, Hua J, Torday JS, Reyes B, Shipp MA (1992) CD10/neutral endopeptidase 24.11 in developing human fetal lung. Patterns of expression and modulation of peptide-mediated proliferation. *J Clin Invest* **90**(6): 2517–2525.

Turner AJ, Tanzawa K (1997) Mammalian membrane metallopeptidases: NEP, ECE, KELL, and PEX. *FASEB J* **11**(5): 355–364.

Zhang Q, Shi S, Yen Y, Brown J, Ta JQ, Le AD (2010) A subpopulation of CD133(+) cancer stem-like cells characterized in human oral squamous cell carcinoma confer resistance to chemotherapy. *Cancer Lett* **289**(2): 151–160.

This work is published under the standard license to publish agreement. After 12 months the work will become freely available and the license terms will switch to a Creative Commons Attribution-NonCommercial-Share Alike 3.0 Unported License.

Supplementary Information accompanies this paper on British Journal of Cancer website (http://www.nature.com/bjc)

FULL PAPER

BJC

British Journal of Cancer (2014) 111, 1572–1580 | doi: 10.1038/bjc.2014.454

Keywords: microRNA; miR-1246; CCNG2; chemoresistance; cancer stem cell; pancreatic cancer

MicroRNA-1246 expression associated with CCNG2-mediated chemoresistance and stemness in pancreatic cancer

S Hasegawa[1,2], H Eguchi[1], H Nagano[1], M Konno[2], Y Tomimaru[1], H Wada[1], N Hama[1], K Kawamoto[1], S Kobayashi[1], N Nishida[2], J Koseki[3], T Nishimura[4], N Gotoh[4], S Ohno[5], N Yabuta[5], H Nojima[5], M Mori[1], Y Doki[1] and H Ishii[*,2,3]

[1]Department of Gastroenterological Surgery, Osaka University, Graduate School of Medicine, 2-2, Yamadaoka, Suita, Osaka 565-0871, Japan; [2]Department of Frontier Science for Cancer and Chemotherapy, Osaka University, Graduate School of Medicine, 2-2, Yamadaoka, Suita, Osaka 565-0871, Japan; [3]Department of Cancer Profiling Discovery, Osaka University, Graduate School of Medicine, 2-2, Yamadaoka, Suita, Osaka 565-0871, Japan; [4]Division of Molecular Therapy, Molecular Targets Laboratory, Institute of Medical Science, University of Tokyo, 4-6-1, Shirokanedai, Minato-ku, Tokyo 108-8639, Japan and [5]Department of Molecular Genetics, Research Institute for Microbial Diseases, Osaka University, 3-1, Yamadaoka, Suita, Osaka 565-0871, Japan

Background: Pancreatic cancer has a poor prognosis because of its high refractoriness to chemotherapy and tumour recurrence, and these properties have been attributed to cancer stem cells (CSCs). MicroRNA (miRNA) regulates various molecular mechanisms of cancer progression associated with CSCs. This study aimed to identify the candidate miRNA and to characterise the clinical significance.

Methods: We established gemcitabine-resistant Panc1 cells, and induced CSC-like properties through sphere formation. Candidate miRNAs were selected through microarray analysis. The overexpression and knockdown experiments were performed by evaluating the *in vitro* cell growth and *in vivo* tumourigenicity. The expression was studied in 24 pancreatic cancer samples after laser captured microdissection and by immunohistochemical staining.

Results: The *in vitro* drug sensitivity of pancreatic cancer cells was altered according to the miR-1246 expression via *CCNG2*. *In vivo*, we found that miR-1246 could increase tumour-initiating potential and induced drug resistance. A high expression level of miR-1246 was correlated with a worse prognosis and CCNG2 expression was significantly lower in those patients.

Conclusions: miR-1246 expression was associated with chemoresistance and CSC-like properties via CCNG2, and could predict worse prognosis in pancreatic cancer patients.

Pancreatic cancer has the worst prognosis of any major malignancy and is the fourth most common cause of cancer death each year in the United States. Even if it is diagnosed at an operable stage and curative resection is achieved, there is still a high incidence of recurrence (Hoyert *et al*, 2006). Although gemcitabine (GEM)-based chemotherapy has formed the core of multimodal therapy for pancreatic cancer (Oettle *et al*, 2007), it is rarely curative and only modestly effective against tumour recurrence. Cancer stem cells (CSCs) have been implicated in the clinical refractoriness, metastasis, and tumour recurrence of various types of cancer, including pancreatic cancer (Hermann *et al*, 2007; Li *et al*, 2007). The molecular mechanisms that link chemoresistance with CSCs remain unclear. Clarifying these mechanisms could improve prognosis of patients with pancreatic cancer.

*Correspondence: Professor H Ishii; E-mail: hishii@gesurg.med.osaka-u.ac.jp

Revised 13 July 2014; accepted 16 July 2014; published online 12 August 2014

© 2014 Cancer Research UK. All rights reserved 0007 – 0920/14

The miRNAs are endogenous, 18–25-bp, single-stranded, non-coding modulators of the post-transcriptional process (Bartel, 2009). In the present study, we focused on miRNAs of GEM-resistant pancreatic cancer cell lines and CSC-like cell populations using sphere formation assays (Pastrana *et al*, 2011); pancreatic CSCs could be enriched as spheroid cells (Hermann *et al*, 2007). We performed comprehensive expression profiling of miRNAs in order to indentify the candidate miRNA and determine its clinical significance.

MATERIALS AND METHODS

Vector constructs and lentiviral production. The lentiviral pLenti-III-miR-1246 vector and its empty pLenti-III vector (Applied Biological Materials Inc., Richmond, Canada) were co-transfected with pCAG-HIVgp and pCMV-VSV-G-RSV-Rev into 293Ta cells (Gene Copoeia Inc., Rockville, MD, USA). Panc1 cells were infected with lentivirus and selected using 1 $\mu g\,ml^{-1}$ puromycin for 4 weeks, to establish stable miR-1246 (Panc1-P-l-OE) and control (Panc1-P-l-C) transfectants. The *CCNG2* lacking miR1246 target sites in 3′UTR were transfected into the Panc1-P-l-OE cells using FuGENE 6 Reagent (Promega, Madison, WI, USA).

Ethics statement on animals. All animal work was performed according to Animal Experiments Committee, Osaka University (the approval number, 24-122-011).

Animal experiments. Four different numbers of Panc1 cells, 1×10^2, 1×10^3, 1×10^4, and 1×10^5, were injected subcutaneously in 4- to 6-week-old female non-obese mice with diabetes/severe combined immunodeficiency (CLEA Japan, Tokyo, Japan). The mice were administered GEM intraperitoneally three times on days 35, 42, and 49 using the once-a-week protocol as to closely replicate clinical use. Mice were given 125 $mg\,kg^{-1}$ GEM, or phosphate-buffered saline as control (Lonardo *et al*, 2011). The tumour volume was calculated as: (longest diameter) × (shortest diameter)^2 × 0.5. The therapy was initiated when the tumour volumes were 60–100 mm^3. The tumours were resected on day 53 after the cell injection. Total RNA was extracted from tumours. Immunohistochemistry was performed using polyclonal goat anti-human cyclinG2 antibody (Santa Cruz Biotechnology Inc., Santa Cruz, CA, USA).

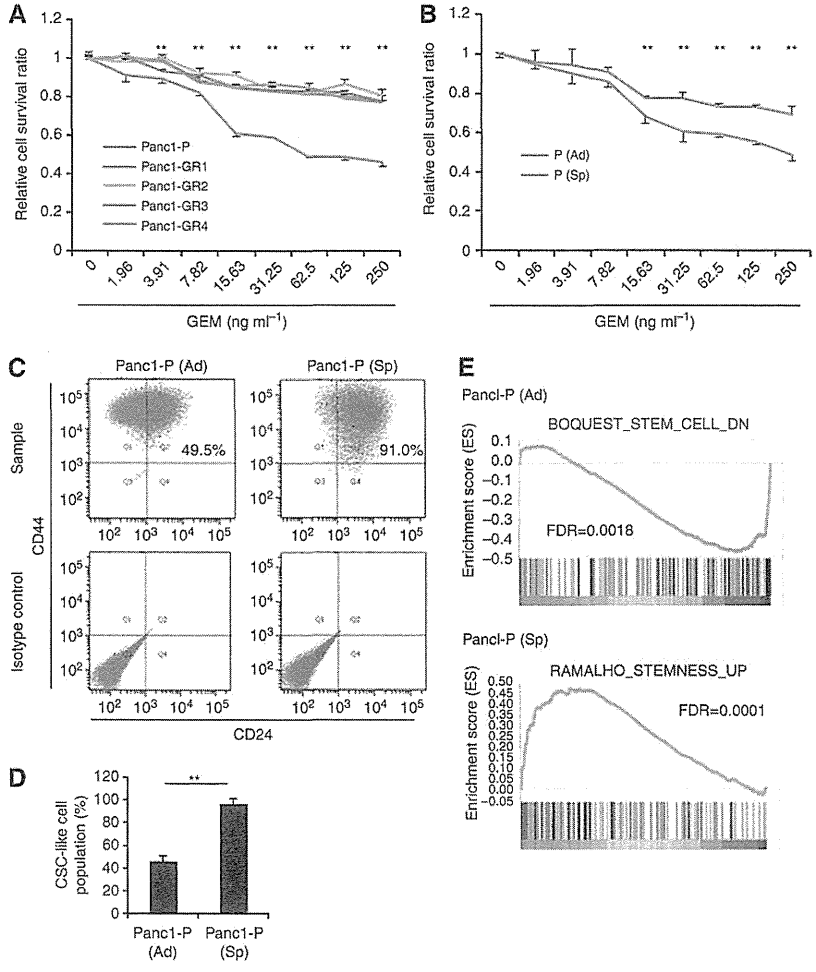

Figure 1. Features of gemcitabine (GEM)-resistant pancreatic cancer cells (Panc1-GRs) and Panc1 parental CSC-like spheroid cells (Panc1-P (Sp)). (**A**) Growth-inhibitory effects of GEM on Panc1 parental (Panc1-P) cells and Panc1-GR (GR1, GR2, GR3, and GR4) cells were assessed by MTT assay. (**B**) Growth-inhibitory effects of GEM on normal adherent condition Panc1-P (Ad) and Panc1-P (Sp) cells were assessed by MTT assay. (**C**) The representative data of flow cytometry showed the CSC-like cell population of Panc1-P in Panc1-P (Ad) cells (left panel) and Panc1-P (Sp) cells (right panel). (**D**) The percentages of the CSC-like cell populations were shown in Pan1-P (Ad) and -P (Sp) cells. This assay was performed three times. (**E**) Gene set enrichment analysis (GSEA) of Panc1-P (Sp) cells compared with Panc1-P (Ad) cells was performed. GSEA-extracted representative gene sets enriched in those cells are shown. Data represent mean ± s.d. of more than three experiments; $^{**}P<0.01$.

Ethics statement on clinical samples. The use of resected samples was approved by the Human Ethics Review Committee of the Graduate School of Medicine, Osaka University (approval number 08226). Written informed consent was obtained from all patients included in the study.

Study on primary tumour samples. Between March 2007 and December 2010, 24 consecutive patients with pancreatic cancer were treated by histologically curative resection (R0) at Osaka University Hospital, and no preoperative therapy was given (Supplementary Table 3). Among 24 patients, 12 patients received adjuvant GEM chemotherapy. Immunohistochemical staining protocol is shown in the Supplementary Materials and Methods. To separate epithelial and mesenchymal parts, laser captured microdissection (LCM; LMD7000, Leica Microsystems GmbH, Wetzlar, Germany) was performed as 8-μm-thick sections from formalin-fixed paraffin-embedded (FFPE) samples. Total RNA was extracted using RNeasy FFPE Kit (Qiagen, Tokyo, Japan). The relative quantification of miRNA was studied by qRT–PCR using comparative CT method ($2^{-\Delta CT}$). Data were normalised using endogenous RNU48 control.

Statistical analysis. The clinicopathological parameters were compared using the Fisher's exact test, and the continuous variables were compared using the Student's *t*-test. The survival curves were computed using the Kaplan–Meier method. Statistical analysis was performed using JMP software version 10.0.2 (SAS Institute Inc., Cary, NC, USA).

RESULTS

Establishment of GEM-resistant pancreatic cancer cell clones. We established four independent GEM-resistant clones of Panc1 cells. Compared with the Panc1-P cells, the Panc1-GR cells were significantly more resistant to GEM (Figure 1A) and showed significantly more drug resistance to 5-FU at three densities (Supplementary Figure 1A). Several studies have recently reported that representative surface markers, such as CD44 + CD24 +, were useful to enrich the CSC-like cells from others in pancreatic cancer cell lines (Hermann *et al*, 2007; Li *et al*, 2007). Flow cytometry analysis of the CSC population in Panc1-GRs revealed that the CD44 + CD24 + population was slightly increased (Figure 1B and Supplementary Figure 1B).

Establishment of pancreatic CSC-like chemoresistant cells. The sphere formation and growth assays revealed that Panc1-P (Sp) was significantly resistant to GEM and 5-FU compared with Panc1-P (Figure 1B and Supplementary Figure 1D). Note that Panc1-P (Sp) cells were chemoresistant to GEM and 5-FU, although not exposed to agents. Flow cytometry analysis revealed

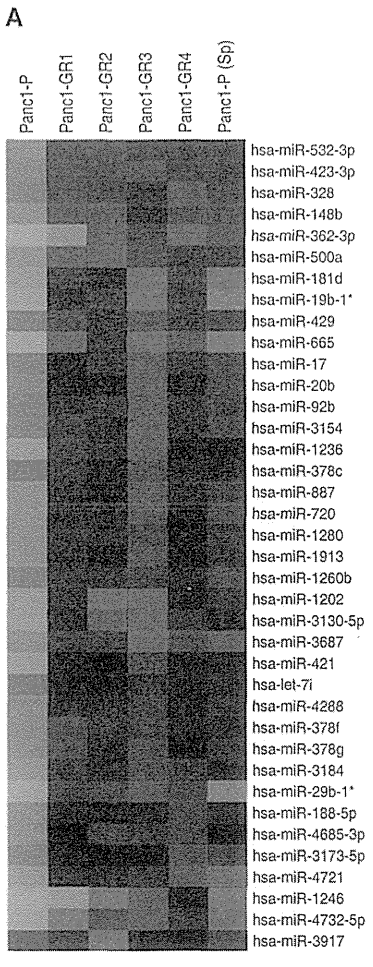

B

	miRNA number	GR/P	P (Sp)/P	Average
1	hsa-miR-1246	2.84	14.13	8.46
2	hsa-miR-720	2.59	1.77	2.18
3	hsa-miR-1280	2.42	1.93	2.18
4	hsa-let-7i	1.88	2.04	1.96
5	hsa-miR-20b	2.17	1.66	1.92
6	hsa-miR-4787-5p	1.54	2.13	1.84
7	hsa-miR-1260b	2.07	1.53	1.80
8	hsa-miR-1908	1.81	1.77	1.79
9	hsa-miR-17	2.02	1.52	1.78
10	hsa-miR-4284	1.74	1.69	1.72
11	hsa-miR-2861	1.67	1.73	1.70
12	hsa-let-7d	1.89	1.50	1.70
13	hsa-miR-106a	1.83	1.50	1.67
14	hsa-miR-4466	1.62	1.65	1.64
15	hsa-miR-3621	1.53	1.71	1.62

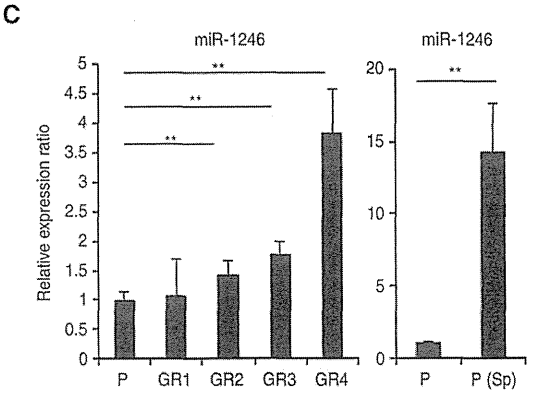

Figure 2. miRNA microarray analysis and the ranking of candidate miRNAs. (A) The heat map revealed the miRNAs whose expression levels were altered >1.5-fold relative to Panc1-P both in Panc1-GRs and -P (Sp) cells. *non-functional miRNA. (B) The list showed the ranking of candidate miRNAs according to the ratio of the change in expression level. From the above 38 miRNAs (A), 15 miRNAs were selected. (C) Real-time qRT–PCR showed the expression of miR-1246 in Panc1-P, -GRs, and -P (Sp) cells. Data represent mean ± s.d. of more than three experiments; $^{**}P<0.01$.

that the CD24 + CD44 + population nearly doubled due to sphere formation (Figure 1C and D).

Gene sets enriched in spheroid cells and adherent cells. Gene set enrichment analysis (GSEA) was performed between the coding gene expression profiles of the spheroid parental Panc1 (Panc1-P (Sp)) cells and those of the adherent parental cells (Panc1-P). The GSEA in spheroid cells revealed upregulation of stem cell pathway and downregulation of adherent pathway (Figure 1E and Supplementary Figure 2A and B).

Outstanding expression of miR-1246 revealed by miRNA microarray analysis. To identify the candidate miRNAs related to chemoresistance and cancer stemness, we performed miRNA microarray studies. The data showed that, among the 1719 miRNAs, the miRNA expression levels of 92 in the Panc1-GR

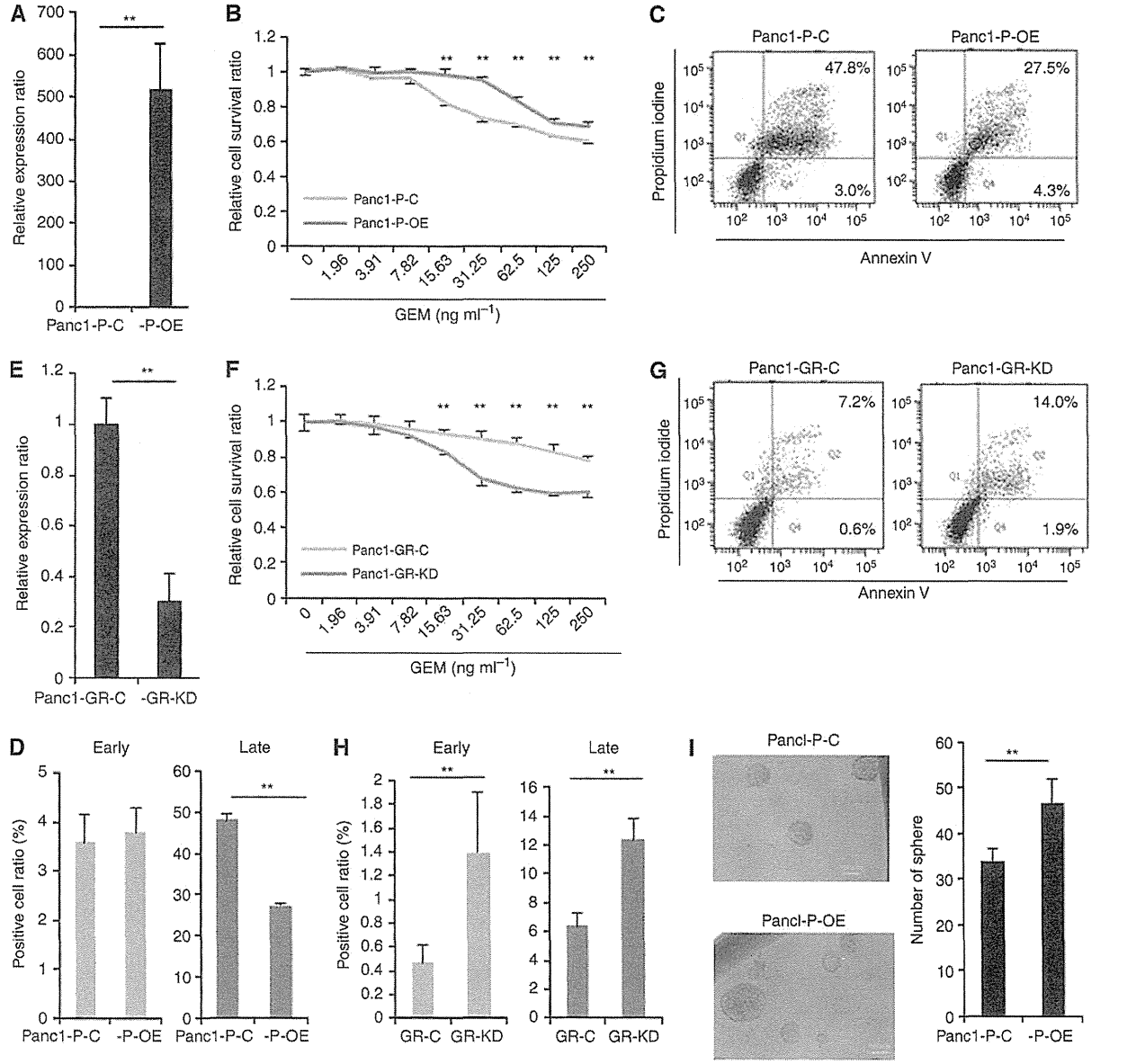

Figure 3. Association of miR-1246 expression with the resistance to GEM and sphere-forming ability. (A) Real-time qRT–PCR showed the expression level of miR-1246 in Panc1-P cells transfected with pre-miR-1246 (Panc1-P-OE) and transfected with the negative control (Panc1-P-C). (B) MTT assay demonstrated relative cell survival ratio of Panc1-P-C and Panc1-P-OE cells to GEM, respectively. (C) The representative data of Annexin V assay showed the distribution of the early and late apoptotic cells in the Panc1-P-C and Panc1-P-OE cells after GEM exposure for 72 h. (D) The percentages of early and late apoptotic cells in the Panc1-P-C and Panc1-P-OE cells after GEM exposure for 72 h. This assay was performed three times. (E) Real-time qRT–PCR showed the expression level of miR-1246 in Panc1-GR cells transfected with anti-miR-1246 (Panc1-GR-KD) and transfected with negative control (Panc1-GR-C). (F) MTT assay demonstrated relative cell survival ratio of Panc1-GR-C and Panc1-GR-KD to GEM. (G) The representative data of Annexin V assay showed the distribution of the early and late apoptotic cells in Panc1-GR-C and Panc1-GR-KD cells after GEM exposure for 72 h. (H) The percentages of early and late apoptotic cells in Panc1-GR-C and Panc1-GR-KD cells after GEM exposure for 72 h. This assay was performed three times. (I) Sphere formation assay was performed in Panc1-P-C and Panc1-P-OE cells. The representative image of spheres (left) and the number of spheres (right) were shown. Bar = 100 μm. Data represent mean ± s.d. of three experiments; $^{**}P<0.01$.

cells (Supplementary Table 1) and 216 in the Panc1-P (Sp) cells (Supplementary Table 2) were altered by an average of >1.5-fold relative to the parental levels. The heat map showed 38 common miRNAs, which included 37 miRNAs (>1.5-fold) and 1 miRNA (<0.66-fold) of the parental levels (Figure 2A). By excluding 23 miRNAs that showed undetectable or extremely low expression and non-functional miRNAs, we found 15 candidate miRNAs were expressed strongly in both Panc1-GRs and Panc1-P (Sp) cells (Figure 2B). miR-1246 showed the highest alteration (8.46 average fold change: 14.13-fold increase in the Panc1-P (Sp) and 2.84-fold increase in the Panc1-GR). The fold change of the miR-1246 expression level was outstanding in Panc1-P (Sp) cells. The real-time qRT–PCR confirmed the miR-1246 upregulation in Panc1-GRs and -P (Sp) cells (Figure 2C). We then assessed miR-1246 for further analysis.

Association of miR-1246 expression with the resistance to GEM and sphere-forming ability. To evaluate the effect of miR-1246 on the response to GEM in Panc1 cells, pre- or anti-miR-1246 was introduced into Panc1-P/-GR4. Real-time qRT–PCR confirmed that the transfection with pre-miR-1246 resulted in the marked overexpression of mature miR-1246 (Panc1-P-OE; Figure 3A). The proliferation rate of the Panc1-P-OE cells was slightly increased compared with control Panc1-P-C. The MTT assay demonstrated that transfection of pre-miR-1246 into Panc1-P resulted in resistance to GEM (Figure 3B). In contrast, anti-miR-1246 transfection into Panc1-GR4, whose endogenous levels of miR-1246 was 3.5-fold higher than that of Panc1-P (Figure 2C), resulted in sufficient inhibition of miR-1246 by qRT–PCR (Panc1-GR-KD; Figure 3E). MTT assay demonstrated a significant reduction of chemoresistance to GEM in the Panc1-GR-KD cells (Figure 3F). The proliferation rate of the Panc1-GR-KD cells was not changed compared with control Panc1-GR-C. These results indicated that miR-1246 induced GEM-resistance in Panc1 cells. We assessed the sphere-forming ability. The proliferation ratio of spheres in Panc1-P-OE was significantly higher than that in Panc1-P-C (Supplementary Figure 1C). Panc1-P-OE spheres increased compared to Panc1-P-C (Figure 3I). We confirm the results with

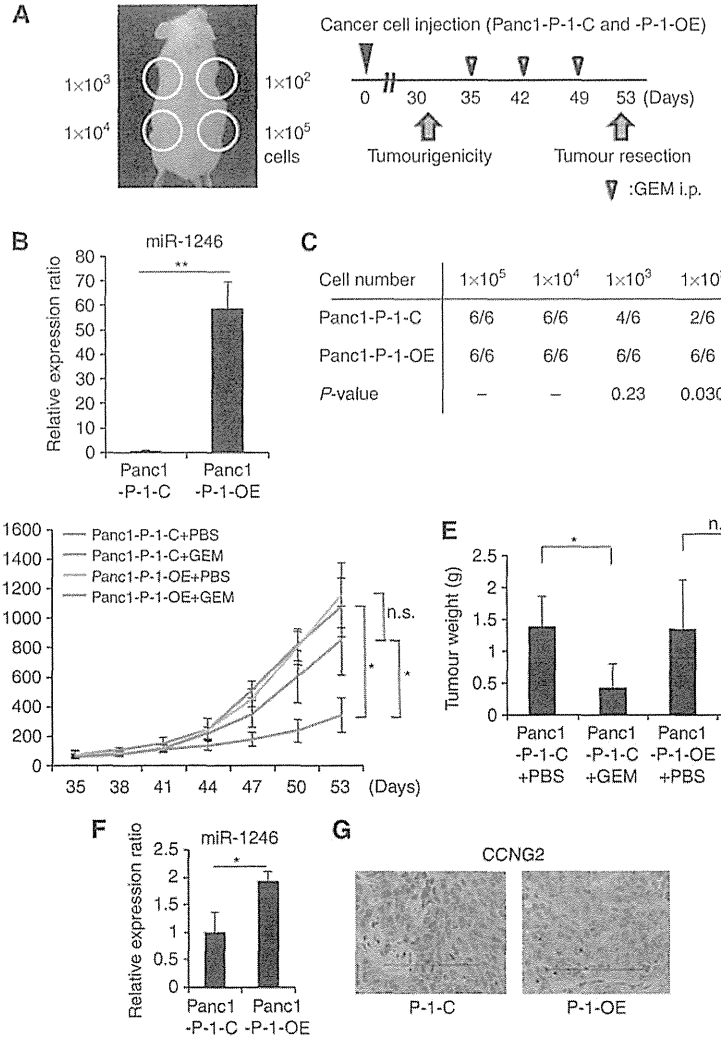

Figure 4. The function of miR-1246 in tumourigenicity and GEM-resistance *in vivo*. (**A**) The experimental design was shown. (**B**) Real-time qRT–PCR showed the expression level of miR-1246 in miR-1246 continuously expressing Panc1 (Panc1-P-I-OE) and control Panc1 (Panc1-P-I-C) cells. (**C**) The tumourigenic ability was evaluated on day 30 after Panc1 cell injection in the Panc1-P-I-C and Panc1-P-I-OE groups. (**D**) The therapy was initiated when the tumour volumes (1×10^5 cells injected) were between 60 and 100 mm^3. (**E**) The weights of tumours were measured at day 53 after resection. (**F**) Real-time qRT–PCR showed the expression level of miR-1246 in the tumours of Panc1-P-I-OE and Panc1-P-I-C cell-injected groups. (**G**) Immunohistochemistry of the tumour specimens showed *CCNG2* expression in the tumours of Panc1-P-I-OE and Panc1-P-I-C cell-injected groups. Bar = 100 μm. Data represent mean ± s.d. of three experiments; $^*P<0.05$; $^{**}P<0.01$.

another pancreatic cancer cell line, MiaPaCa2 with endogenous miR-1246 decreased (40% of Panc1; Supplementary Figure 4A). The pre-miR-1246 transfection resulted in replenishment of miR-1246 (Supplementary Figure 4C). The MTT assay demonstrated that miR-1246 anti-sensitised MiaPaCa2 to GEM treatment (Supplementary Figure 4E). Although CSC-like cell population was relatively rare (Supplementary Figure 4B), the miR-1246 OE (Sp) enriched by sphere assay revealed that the proliferation rate was higher than control cells (Supplementary Figure 4D). The miR-1246 OE sphere increased significantly compared to control (Supplementary Figure 4F).

miR-1246 induced tumourigenicity and refractoriness to GEM. Although pre-miR-1246 expression continued for a week, it decreased gradually (Supplementary Figure 3A; the data of anti-miR-1246 in Supplementary Figure 3B). To assess miR-1246 functions relating to tumourigenicity and refractoriness to GEM *in vivo* (Figure 4A), we established Panc1 (Panc1-P-l-OE) cells that overexpressed miR-1246 continuously in high level (Supplementary Figure 3C). We confirmed that the expression level of miR-1246 in Panc1-P-l-OE was ~50-fold higher than that in Panc1-l-C (Figure 4B). The tumourigenicity of Panc1-P-l-OE was significantly increased compared with Panc1-P-l-C (at 1×10^2 cell injection; Figure 4C). The tumour volume and weight of Panc1-P-l-C, but not Panc1-P-l-OE, was significantly inhibited by GEM treatment compared with controls at day 53 (Figure 4D and E). The miR-1246 expression in the Panc1-P-l-OE tumours was significantly two times higher than the expression in Panc1-P-l-C at day 53 (Figure 4F).

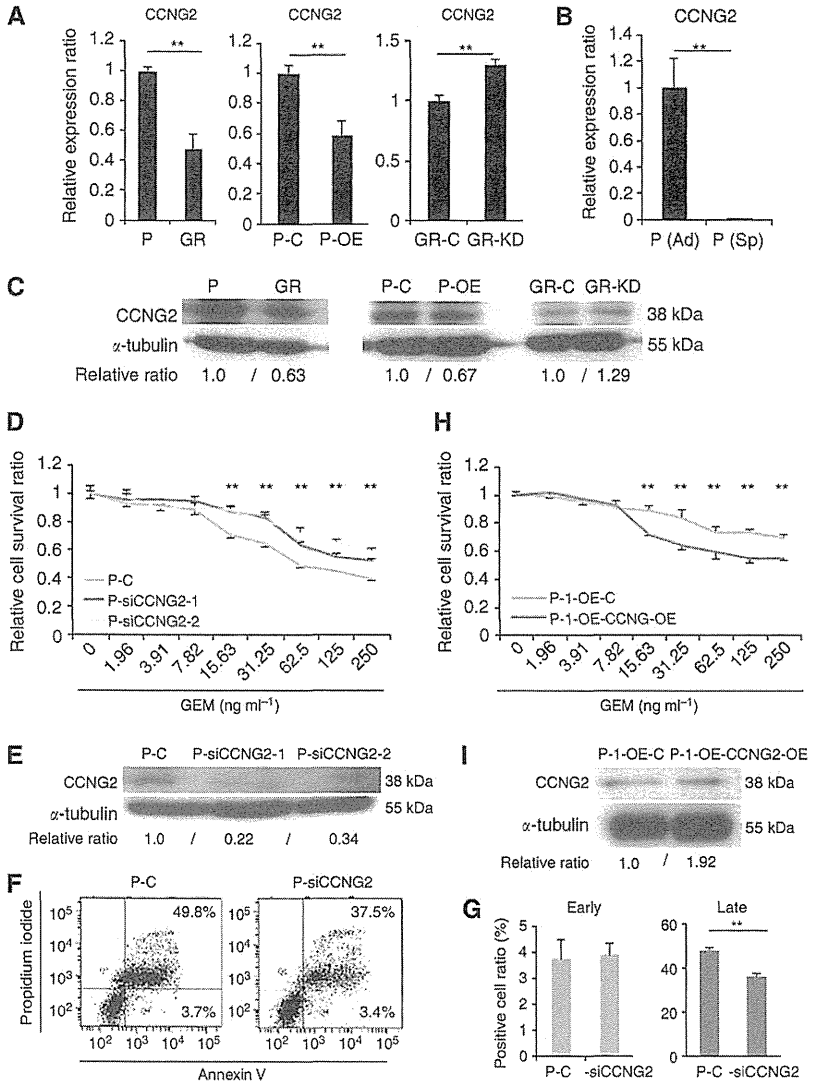

Figure 5. The *CCNG2* function as a target of miR-1246 in Panc1 cells. (**A–C**) Real-time qRT–PCR and western blotting demonstrated *CCNG2* expression level in Panc1-P and Panc1-GR cells, Panc1-P-C and Panc1-P-OE cells, Panc1-GR-C and Panc1-GR-KD cells, and Panc1-P (Ad) and Panc1-P (Sp) cells. (**D**) MTT assay demonstrated the relative cell survival ratio of Panc1-P cells transfected with siCCNG2 (Panc1-P-siCCNG2-1, -2) and transfected with negative control (Panc1-P-C). (**E**) The protein level of *CCNG2* in Panc1-P and GR cells, Panc1-P-C and Panc1-P-OE cells, and Panc1-GR-C and Panc1-GR-KD cells in western blotting. (**F**) The representative data of Annexin V assay showed the distribution of the early and late apoptotic cells in Panc1-P-C and Panc1-P-siCCNG2 after GEM exposure for 72 h. (**G**) The percentages of early and late apoptotic cells in Panc1-P-C and Panc1-P-siCCNG2 after GEM exposure for 72 h. This assay was performed three times. (**H**) MTT assay demonstrated relative cell survival ratio of Panc1-P-l-OE cells transfected with ectopic *CCNG2* (Panc1-P-l-OE-CCNG2-OE) and transfected with control vector (Panc1-P-l-OE-C) to GEM. (**I**) Western blotting demonstrated *CCNG2* expression level in Panc1-P-l-OE-CCNG2-OE and Panc1-P-l-OE-C. Data represent mean ± s.d. of three experiments; $^{**}P<0.01$.

miR-1246 inhibits response to GEM by targeting CCNG2. Few studies have reported miR-1246 expression in gastrointestinal cancers, and little is known about the function. As putative miR-1246 targets, the TargetScan (http://www.targetscan.org/) predicted 178 genes. Among them, *CCNG2*, a family of cyclins that is homologous to CCNG1 (Bates *et al*, 1996) and is also known as a tumour suppressor, was selected for further analysis. Western blotting and qRT–PCR showed that *CCNG2* expression was lower in Panc1-GR cells than in Panc1-P cells (Figure 5A and C). Western blotting and qRT–PCR confirmed that pre-miR-1246 transfection decreased *CCNG2* expression, whereas anti-miR-1246 increased it (Figure 5A and C), suggesting that *CCNG2* was one of the target genes of miR-1246. *CCNG2* expression was significantly lower in Panc1-P (Sp) than in control (Figure 5B). We are interested in a role of *CCNG2* in the resistance to GEM. To this end, we performed knockdown of *CCNG2* by siRNA. Western blotting confirmed the knockdown (Figure 5E). The MTT assay demonstrated that transfection of siCCNG2 elicited the resistance of Panc1-P to GEM (Figure 5D). Given reportedly *CCNG2* regulated cell growth and induced apoptosis (Kim *et al*, 2004), we studied the involvement of apoptosis in present case. In Panc1-P, pre-miR-1246 significantly reduced the number of late apoptotic cells (Figure 3C and D). Similarly, pre-miR-1246 significantly reduced the early and late apoptosis in MiaPaCa2 cells (Supplementary Figure 4G and H). In contrast, the anti-miR-1246 increased the number of early and late apoptotic cells significantly in Panc1-GR (Figure 3G and H). Also, siCCNG2 significantly reduced late apoptosis (Figure 5F and G). These data suggested that miR-1246 regulated chemoresistance via *CCNG2* expression that was involved in apoptosis. Furthermore, in order to study whether the ectopic *CCNG2* expression can rescue the miR-1246-driven GEM-resistance, we transfected *CCNG2* vector (lacking miR-1246 target sites) into Panc1-P-l-OE cells. The MTT assay demonstrated that ectopic *CCNG2* significantly reduced chemoresistance to GEM in the Panc1-P-l-OE cells (Figure 5H); the elevation of *CCNG2* expression was confirmed with western blotting (Figure 5I).

As for the *in vivo* experiment mentioned above, qRT–PCR and immunohistochemistry demonstrated that the *CCNG2* expression was decreased in both the mRNA (data not shown) and protein levels (Figure 4G) in the Panc1-P-l-OE tumours at day 53. This result supported the conclusion that *CCNG2* was one of the target genes for miR-1246.

miR-1246 and CCNG2 expression in primary pancreatic cancer samples. To study the clinical significance, we performed LCM to collect cancer sections from tumour tissues, qRT–PCR, and immunohistochemistry in 24 patients who underwent R0 resection

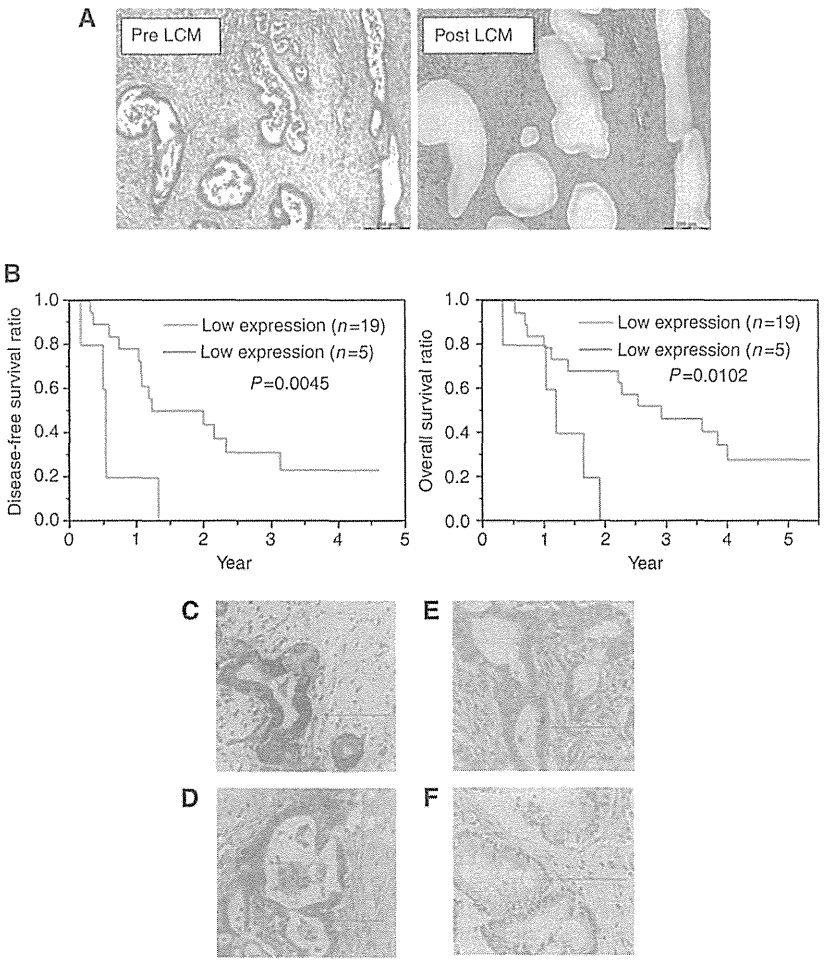

Figure 6. miR-1246 and *CCNG2* expression in primary pancreatic cancer samples. (**A**) The representative image of pre/post (left/right) laser captured microdissection (LCM). Bar = 200 μm. (**B**) Relationships between miR-1246 expression and disease-free survival, or overall survival. (**C–F**) Immunohistochemical staining of *CCNG2* in 24 primary tumours. The *CCNG2*-positive cases show the diffuse (**C**) or spotted (**D**) nuclear patterns; *CCNG2*-negative ones depict cytoplasmic pattern (**E**; not stained in the nucleus) or the negative pattern (**F**; not stained in the nucleus or cytoplasm).

Table 1. The primary pancreatic cancer patients in the present study

	miR-1246 expression		
	Low ($n=19$)	High ($n=5$)	*P*-value
Age (<65:≥65)	7:12	0:5	0.14
Sex (male:female)	12:7	2:3	0.33
Histopathological type (well or mod:poor)	17:2	5:0	0.62
Tumour size (mm)	24.4±14.4	24.6±9.5	0.48
Tumour location (head:body or tail)	8:11	5:0	0.030
Pathological depth of invasion depth pT (T1 or T2:T3)	6:13	0:5	0.20
Pathological lymph node metastasis pN (negative:positive)	12:7	1:4	0.14
Pathological stage (IA or IB or IIA:IIB or IV)	12:7	1:4	0.14
Adjuvant therapy (−/+)	9:10	2:3	0.59
CCNG2 expression (negative:positive)	5:14	4:1	0.047

Abbreviations: mod = moderately differentiated; poor = poorly differentiated; well = well differentiated.

(Figure 6A). The expression level of miR-1246 in each sample was shown in Supplementary Figure 5A. Of the 24 patients, the mean expression level of miR-1246 was 57.5 (/RNU48). We divided those patients into two groups by the mean value of miR-1246 expression (high or low). Disease-free survival ratio ($P=0.0045$) and overall survival ratios ($P=0.0102$) were significantly lower in the high miR-1246 expression group (Figure 6B).

Subsequently, immunohistochemical staining for *CCNG2* was performed in the corresponding 24 samples. The nuclei of normal pancreatic ductal cells were partially stained and the acinar cells were stained strongly in the cytoplasm and nuclei, which were used as positive controls (Supplementary Figure 5B and C). With cancer sections, although *CCNG2* had been shown to appear not only in the nucleus but also in the cytoplasm, the functional *CCNG2* protein may localise in the nucleus (Choi *et al*, 2009). We defined *CCNG2*-positive cases as those that showed diffuse or spotted nuclear patterns (Figure 6C and D), and *CCNG2*-negative cases as cytoplasmic pattern (not stained in the nucleus; Figure 6E) or an absent pattern (not stained in the nucleus or cytoplasm; Figure 6F) in pancreatic cancer lesions. Among the 24 patients examined, 15 (62.5%) showed positive staining, whereas 9 (37.5%) patients were negative for *CCNG2*.

Finally, we evaluated the patient backgrounds in low or high miR-1246 expression groups (Table 1 and Supplementary Table 3). The tumour location and *CCNG2* expression in other clinicopathological factors showed significant difference between the two groups. The high miR-1246 expression group showed lower *CCNG2* expression, whereas the low miR-1246 expression group showed high *CCNG2* expression, with statistical significance ($P=0.047$). This result demonstrated that miR-1246 expression correlated inversely with *CCNG2* expression in clinical samples, and an especially high expression level of miR-1246 predicted worse pancreatic cancer prognosis.

DISCUSSION

Several miRNAs were reported in association with drug resistance against GEM: miR-15a (Zhang *et al*, 2010), miR-21 (Ali *et al*, 2010; Giovannetti *et al*, 2010), miR-200b and miR-200c (Ali *et al*, 2010; Li *et al*, 2009), miR-320c (Iwagami *et al*, 2013), and members of the let7 family (Li *et al*, 2009). Although these reports studied the bulk of tumours, we here identified chemoresistance- and cancer stemness-associated miRNAs. We focused on miR-1246, which was expressed in CSC-like spheroid cells. CSC-like spheroids showed chemoresistance for reagents, and the gene microarray analysis and GSEA revealed that the stemness-related pathways were increased, suggesting that the spheroids at least partially mimicked the CSC-like phenotype.

miR-1246 was reported as a diagnostic biomarker for oesophageal squamous cell carcinoma (Takeshita *et al*, 2013) and cervical cancer (Chen *et al*, 2014). However, few studies have reported the miR-1246 function in pancreatic cancer. In the present study, we demonstrated that miR-1246 induced chemoresistance and was related to cancer stemness in pancreatic cancer cell lines. Among miR-1246 targets, we focused on *CCNG2* (Bates *et al*, 1996), a tumour suppressor gene. The *CCNG2* expression was down-regulated in the thyroid (Ito *et al*, 2003), oral (Kim *et al*, 2004), breast (Montagner *et al*, 2012), gastric (Sun *et al*, 2014a), oesophageal (Chen *et al*, 2013), prostate (Cui *et al*, 2014a), kidney (Cui *et al*, 2014b), and colorectal (Sun *et al*, 2014b) cancers. Antitumor agents induced *CCNG2* expression and inhibited cancer (Kasukabe *et al*, 2008; Padua and Hansen, 2009; Zhao *et al*, 2011). We demonstrated that *CCNG2* was decreased in pancreatic CSC-like spheroid cells and induced apoptosis, similarly to oral cancer (Kim *et al*, 2004). Given that *CCNG2* deeply participated in cancer proliferation, invasion, chemoresistance, and differentiation, which characterise CSCs, *CCNG2* may be involved at least partially in the maintenance of CSC-like spheroid cells. The present data showed *CCNG2* expression was correlated inversely with miR-1246 expression, suggesting miR-1246 control *CCNG2* function. We confirmed *in vitro* data by human primary tumours. Laser captured microdissection analysis and immunohistochemistry revealed the high miR-1246 expression and low *CCNG2* expression in patients. The present study suggested that miR-1246-*CCNG2* axis is critical for chemoresistance, and shows the candidacy as a *bona fide* useful predictive marker.

ACKNOWLEDGEMENTS

We thank the members of our laboratories for their fruitful discussion. This work was supported in part by a Grant-in-Aid for Scientific Research and a grant from the Platform for Drug Discovery, Informatics, and Structural Life Science from the Ministry of Education, Culture, Sports, Science and Technology; a Grant-in-Aid from the Third Comprehensive 10-year Strategy for Cancer Control, Ministry of Health, Labor, and Welfare; a grant from the Kobayashi Cancer Research Foundation; a grant from the Princess Takamatsu Cancer Research Fund, Japan; a grant from the National Institute of Biomedical Innovation, Japan.

CONFLICT OF INTEREST

HI and MK received partial support from Chugai Co., Ltd., Yakult Honsha Co., Ltd., and Merck Co., Ltd. through institutional endowments.

REFERENCES

Ali S, Ahmad A, Banerjee S, Padhye S, Dominiak K, Schaffert JM, Wang Z, Philip PA, Sarkar FH (2010) Gemcitabine sensitivity can be induced in pancreatic cancer cells through modulation of miR-200 and miR-21 expression by curcumin or its analogue CDF. *Cancer Res* **70**: 3606–3617.

Bartel DP (2009) MicroRNAs: target recognition and regulatory functions. *Cell* **136**: 215–233.

Bates S, Rowan S, Vousden KH (1996) Characterisation of human cyclin G1 and G2: DNA damage inducible genes. *Oncogene* **13**: 1103–1109.

Chen J, Yao D, Zhao S, He C, Ding N, Li L, Long F (2014) MiR-1246 promotes SiHa cervical cancer cell proliferation, invasion, and migration through suppression of its target gene thrombospondin 2. *Arch Gynecol Obstet* (in press).

Chen JQ, Liu CJ, Wen HX, Shi CL, Zhang HS, Li M, Sun GG (2013) Changes in the expression of cyclin G2 in esophageal cancer cell and its significance. *Tumour Biol* **35**: 3355–3362.

Choi MG, Noh JH, An JY, Hong SK, Park SB, Baik YH, Kim KM, Sohn TS, Kim S (2009) Expression levels of cyclin G2, but not cyclin E, correlate with gastric cancer progression. *J Surg Res* **157**: 168–174.

Cui DW, Cheng YJ, Jing SW, Sun GG (2014a) Effect of cyclin G2 on proliferative ability of prostate cancer PC-3 cell. *Tumour Biol* **35**: 3017–3024.

Cui DW, Sun GG, Cheng YJ (2014b) Change in expression of cyclin G2 in kidney cancer cell and its significance. *Tumour Biol* **35**: 3177–3183.

Giovannetti E, Funel N, Peters GJ, Del Chiaro M, Erozenci LA, Vasile E, Leon LG, Pollina LE, Groen A, Falcone A, Danesi R, Campani D, Verheul HM, Boggi U (2010) MicroRNA-21 in pancreatic cancer: correlation with clinical outcome and pharmacologic aspects underlying its role in the modulation of gemcitabine activity. *Cancer Res* **70**: 4528–4538.

Hermann PC, Huber SL, Herrler T, Aicher A, Ellwart JW, Guba M, Bruns CJ, Heeschen C (2007) Distinct populations of cancer stem cells determine tumor growth and metastatic activity in human pancreatic cancer. *Cell Stem Cell* **1**: 313–323.

Hoyert DL, Heron MP, Murphy SL, Kung HC (2006) Deaths: final data for 2003. *Natl Vital Stat Rep* **54**: 1–120.

Ito Y, Yoshida H, Uruno T, Nakano K, Takamura Y, Miya A, Kobayashi K, Yokozawa T, Matsuzuka F, Kuma K, Miyauchi A (2003) Decreased expression of cyclin G2 is significantly linked to the malignant transformation of papillary carcinoma of the thyroid. *Anticancer Res* **23**: 2335–2338.

Iwagami Y, Eguchi H, Nagano H, Akita H, Hama N, Wada H, Kawamoto K, Kobayashi S, Tomokuni A, Tomimaru Y, Mori M, Doki Y (2013) miR-320c regulates gemcitabine-resistance in pancreatic cancer via SMARCC1. *Br J Cancer* **109**: 502–511.

Kasukabe T, Okabe-Kado J, Honma Y (2008) Cotylenin A, a new differentiation inducer, and rapamycin cooperatively inhibit growth of cancer cells through induction of cyclin G2. *Cancer Sci* **99**: 1693–1698.

Kim Y, Shintani S, Kohno Y, Zhang R, Wong DT (2004) Cyclin G2 dysregulation in human oral cancer. *Cancer Res* **64**: 8980–8986.

Li C, Heidt DG, Dalerba P, Burant CF, Zhang L, Adsay V, Wicha M, Clarke MF, Simeone DM (2007) Identification of pancreatic cancer stem cells. *Cancer Res* **67**: 1030–1037.

Li Y, VandenBoom 2nd TG, Kong D, Wang Z, Ali S, Philip PA, Sarkar FH (2009) Up-regulation of miR-200 and let-7 by natural agents leads to the reversal of epithelial-to-mesenchymal transition in gemcitabine-resistant pancreatic cancer cells. *Cancer Res* **69**: 6704–6712.

Lonardo E, Hermann PC, Mueller MT, Huber S, Balic A, Miranda-Lorenzo I, Zagorac S, Alcala S, Rodriguez-Arabaolaza I, Ramirez JC, Torres-Ruiz R, Garcia E, Hidalgo M, Cebrian DA, Heuchel R, Lohr M, Berger F, Bartenstein P, Aicher A, Heeschen C (2011) Nodal/Activin signaling drives self-renewal and tumorigenicity of pancreatic cancer stem cells and provides a target for combined drug therapy. *Cell Stem Cell* **9**: 433–446.

Montagner M, Enzo E, Forcato M, Zanconato F, Parenti A, Rampazzo E, Basso G, Leo G, Rosato A, Bicciato S, Cordenonsi M, Piccolo S (2012) SHARP1 suppresses breast cancer metastasis by promoting degradation of hypoxia-inducible factors. *Nature* **487**: 380–384.

Oettle H, Post S, Neuhaus P, Gellert K, Langrehr J, Ridwelski K, Schramm H, Fahlke J, Zuelke C, Burkart C, Gutberlet K, Kettner E, Schmalenberg H, Weigang-Koehler K, Bechstein WO, Niedergethmann M, Schmidt-Wolf I, Roll L, Doerken B, Riess H (2007) Adjuvant chemotherapy with gemcitabine vs observation in patients undergoing curative-intent resection of pancreatic cancer: a randomized controlled trial. *JAMA* **297**: 267–277.

Padua MB, Hansen PJ (2009) Changes in expression of cell-cycle-related genes in PC-3 prostate cancer cells caused by ovine uterine serpin. *J Cell Biochem* **107**: 1182–1188.

Pastrana E, Silva-Vargas V, Doetsch F (2011) Eyes wide open: a critical review of sphere-formation as an assay for stem cells. *Cell Stem Cell* **8**: 486–498.

Sun GG, Hu WN, Cui DW, Zhang J (2014a) Decreased expression of CCNG2 is significantly linked to the malignant transformation of gastric carcinoma. *Tumour Biol* **35**: 2631–2639.

Sun GG, Zhang J, Hu WN (2014b) CCNG2 expression is downregulated in colorectal carcinoma and its clinical significance. *Tumour Biol* **35**: 3339–3346.

Takeshita N, Hoshino I, Mori M, Akutsu Y, Hanari N, Yoneyama Y, Ikeda N, Isozaki Y, Maruyama T, Akanuma N, Komatsu A, Jitsukawa M, Matsubara H (2013) Serum microRNA expression profile: miR-1246 as a novel diagnostic and prognostic biomarker for oesophageal squamous cell carcinoma. *Br J Cancer* **108**: 644–652.

Zhang XJ, Ye H, Zeng CW, He B, Zhang H, Chen YQ (2010) Dysregulation of miR-15a and miR-214 in human pancreatic cancer. *J Hematol Oncol* **3**: 46.

Zhao Z, Liu Y, He H, Chen X, Chen J, Lu YC (2011) Candidate genes influencing sensitivity and resistance of human glioblastoma to Semustine. *Brain Res Bull* **86**: 189–194.

This work is published under the standard license to publish agreement. After 12 months the work will become freely available and the license terms will switch to a Creative Commons Attribution-NonCommercial-Share Alike 3.0 Unported License.

Supplementary Information accompanies this paper on British Journal of Cancer website (http://www.nature.com/bjc)

Role of pyruvate kinase M2 in transcriptional regulation leading to epithelial–mesenchymal transition

Atsushi Hamabe[a,b,1], Masamitsu Konno[b,1], Nobuhiro Tanuma[c], Hiroshi Shima[c], Kenta Tsunekuni[a,d,e], Koichi Kawamoto[a,b], Naohiro Nishida[b], Jun Koseki[e], Koshi Mimori[f], Noriko Gotoh[g], Hirofumi Yamamoto[a], Yuichiro Doki[a,b,e], Masaki Mori[a,b,e,2], and Hideshi Ishii[b,e,2]

Departments of [a]Gastrointestinal Surgery and [b]Frontier Science for Cancer and Chemotherapy, Graduate School of Medicine, Osaka University, Osaka 565-0871, Japan; [c]Division of Cancer Chemotherapy, Miyagi Cancer Center Research Institute, Sendai 981-1293, Japan; [d]Taiho Pharmaceutical Co., Ltd., Chiyoda-ku, Tokyo 101-0054, Japan; [e]Department of Cancer Profiling Discovery, Graduate School of Medicine, Osaka University, Osaka 565-0871, Japan; [f]Department of Surgery, Kyushu University Beppu Hospital, Beppu 874-0838, Japan; and [g]Division of Cancer Cell Biology, Cancer Research Institute of Kanazawa University, Kanazawa 920-1192, Japan

Edited by Carlo M. Croce, The Ohio State University, Columbus, OH, and approved September 25, 2014 (received for review May 2, 2014)

Pyruvate kinase M2 (PKM2) is an alternatively spliced variant of the pyruvate kinase gene that is preferentially expressed during embryonic development and in cancer cells. PKM2 alters the final rate-limiting step of glycolysis, resulting in the cancer-specific Warburg effect (also referred to as aerobic glycolysis). Although previous reports suggest that PKM2 functions in nonmetabolic transcriptional regulation, its significance in cancer biology remains elusive. Here we report that stimulation of epithelial–mesenchymal transition (EMT) results in the nuclear translocation of PKM2 in colon cancer cells, which is pivotal in promoting EMT. Immunoprecipitation and LC-electrospray ionized TOF MS analyses revealed that EMT stimulation causes direct interaction of PKM2 in the nucleus with TGF-β–induced factor homeobox 2 (TGIF2), a transcriptional cofactor repressor of TGF-β signaling. The binding of PKM2 with TGIF2 recruits histone deacetylase 3 to the E-cadherin promoter sequence, with subsequent deacetylation of histone H3 and suppression of E-cadherin transcription. This previously unidentified finding of the molecular interaction of PKM2 in the nucleus sheds light on the significance of PKM2 expression in cancer cells.

pyruvate kinase M2 | epithelial–mesenchymal transition | colorectal cancer | invasion | transforming growth factor-β–induced factor homeobox 2

Colorectal cancer (CRC) is the second most common cancer in the world, with more than 1.2 million new cases and about 600,000 deaths annually (1). Cancerous cells exploit a cancer-specific glycolytic system known as the Warburg effect (also referred to as aerobic glycolysis), which involves rapid glucose uptake and preferential conversion to lactate, despite an abundance of oxygen (2, 3). The precise mechanism underpinning aerobic glycolysis was unclear for a long time. However, in 2008, pyruvate kinase M2 (PKM2) gained attention when its expression was shown to be required for the maintenance of aerobic glycolysis (4). PKM2 is an alternatively spliced variant of the PKM gene that regulates the final rate-limiting step of glycolysis. PKM2 is expressed during embryonic development, but it is generally not expressed in most adult tissues. However, its counterpart, PKM1, is exclusively expressed in adult tissues. PKM2 has been shown to be reactivated in tumor development (5, 6). In cancer cells, PKM2 expression allows the diversion of glycolytic flux into the pentose phosphate pathway associated with attenuated pyruvate kinase activity, thereby meeting the biosynthetic demands for rapid proliferation (3).

Investigations about the nuclear function of PKM2 arose after elucidation of the PKM2 metabolic function. It was identified that in cancer cells, PKM2 can translocate into the nucleus and function as a transcriptional cofactor in response to several extracellular signals, including EGF and hypoxia, subsequently activating CYCLIN D1, C-MYC, or hypoxia-inducible factor 1α (HIF-1α) (7, 8). Particularly in the hypoxic condition, PKM2 interacts with HIF-1α and participates in a positive feedback loop, thereby enhancing HIF-1α transactivation and reprogramming glucose metabolism by regulating the expression of glycolysis-associated enzymes (8). This finding suggested that the PKM2 nuclear function may operate upstream of metabolic regulation and that the resultant metabolic reprogramming and oncogene activation by PKM2 work cooperatively to promote cancer cell proliferation and tumor growth.

In addition to proliferation maintenance and growth suppression prevention, invasion and metastasis have also been targeted as hallmarks of cancer (9). In the invasion process, cancer cells acquire the ability to dissociate from the bulk of the tumor and to migrate into the surrounding stroma, which is regulated by epithelial–mesenchymal transition (EMT) (9, 10). During EMT, cancer cells lose their cell-to-cell contacts by

Significance

Our study shows that pyruvate kinase M2 (PKM2), an alternatively spliced variant of the pyruvate kinase gene, mediates epithelial–mesenchymal transition (EMT), which is critical for cancer cells to acquire invasive potential. Our study demonstrates that EMT stimulates nuclear translocation of PKM2 and decreases epithelial cadherin transcription (a requirement for EMT induction). Our results also demonstrate that PKM2 interacts with the transcriptional factor TGF-β–induced factor homeobox 2, which induces the deacetylation of histone H3, resulting in repressed E-cadherin expression. The precise understanding of nuclear PKM2 function suggests the potential for a model preventing cancer metastasis.

Author contributions: A.H., M.K., K.T., K.K., N.N., J.K., K.M., N.G., H.Y., Y.D., M.M., and H.I. designed research; A.H., M.K., and H.I. performed research; A.H., M.K., N.T., H.S., and H.I. contributed new reagents/analytic tools; A.H., M.K., J.K., N.G., M.M., and H.I. analyzed data; and A.H., M.K., N.T., H.S., K.T., K.K., N.N., J.K., K.M., N.G., M.M., and H.I. wrote the paper.

Conflict of interest statement: This work was supported in part by a Grant-in-Aid for Scientific Research from the Ministry of Education, Culture, Sports, Science, and Technology; a Grant-in-Aid from the Third Comprehensive 10-year Strategy for Cancer Control, Ministry of Health, Labor, and Welfare; a grant from the Kobayashi Cancer Research Foundation; a grant from the Princess Takamatsu Cancer Research Fund, Japan; a grant from the National Institute of Biomedical Innovation; and a grant from the Osaka University Drug Discovery Funds. A.H. is a research fellow of the Japan Society for the Promotion of Science. Partial support was received from Taiho Pharmaceutical Co., Ltd. (to J.K., M.M., and H.I.), Chugai Co., Ltd., Yakult Honsha Co., Ltd., Merck Co., Ltd., Takeda Science Foundation, and Takeda Medical Research Foundation (to M.K., N.N., M.M., and H.I.) through institutional endowments.

This article is a PNAS Direct Submission.

[1]A.H. and M.K. contributed equally to this work.

[2]To whom correspondence may be addressed. Email: mmori@gesurg.med.osaka-u.ac.jp or hishii@gesurg.med.osaka-u.ac.jp.

This article contains supporting information online at www.pnas.org/lookup/suppl/doi:10.1073/pnas.1407717111/-/DCSupplemental.

inhibiting epithelial cadherin (E-cadherin; encoded by *CDH1*) expression and acquiring mesenchymal markers. This process is physiologically important during embryogenesis and is required for in utero development. Given that PKM2 expression and EMT are common to both tumorigenesis and development, PKM2 may affect EMT within cancer cells. However, the significance of PKM2 during EMT or invasion is yet to be investigated.

In the present study, we demonstrate that PKM2 translocates into the nucleus during EMT and acts as a transcription cofactor that inhibits *CDH1* expression. PKM2 interacts with TGF-β–induced factor homeobox 2 (TGIF2), which recruits histone deacetylase 3 (HDAC3) to the promoter sequence of E-cadherin, thereby promoting histone H3 lysine 9 (H3K9) deacetylation and *CDH1* expression down-regulation.

Results

EMT Induction Elicits Nuclear Translocation of PKM2. For the induction of EMT, we cultured colon cancer cells in a medium with TGF-β1 and EGF, as described previously (Fig. 1*A*) (11–14). The SW480 cells changed morphology from epithelial to fibroblastic-like and spindle-shaped in a time-dependent manner (Fig. 1*B*). Consistent with this observation, *CDH1* transcript expression was suppressed, whereas the expression levels of the vimentin (*VIM*), zinc finger e-box binding homeobox 1 (*ZEB1*), and snail family zinc finger 2 (*SNAI2*) genes were increased (Fig. 1*C*). PK gene expression was induced in the EMT condition, with preferential expression of PKM2 compared with PKM1 (Fig. 1*D*). Western blot analysis indicated that the induction of EMT resulted in decreased *CDH1* expression, increased *VIM* expression, and up-regulated PKM2 (Fig. 1*E*). We confirmed that the expression and secretion of endogenous TGF-β1 was minimal in SW480 (Fig. S1 *A* and *B*).

To determine the intracellular localization of proteins, cytoplasmic and nuclear fractions were separated from the EMT-induced cells and Western blot analysis was performed. The data indicated that, although the EMT condition stimulated an increase in cytoplasmic PKM2, nuclear PKM2 was augmented compared with levels in the pre-EMT state (Fig. 1*F*). Immunocytochemistry and immunofluorescence intensity quantification confirmed the increase in nuclear PKM2 (Fig. S2 *A–D*). In addition, we confirmed that nuclear PKM2 was also increased in HCT116 cells under the same EMT condition (Fig. S2*E*) and that the expression of EMT markers was increased in murine *Pkm2* knock-in, compared with *Pkm1* knock-in, mesencymal cells, as well as other human cancer cells (Fig. S1 *C* and *D*).

Previous studies showed that EGF stimulation increased nuclear PKM2 (7) and indicated that cytoplasmic PKM2 functions with tetramer formation, whereas nuclear PKM2 functions with dimer formation. Given that the large hydrophobic hole at the nucleotide binding site is buried in tetrameric PKM2 structure, which becomes accessible in dimer form (15), the dimer formation may provide a protein binding ability. We studied the status of PKM2 during EMT and found that simultaneous stimulation by TGF-β1 and EGF, in comparison with either alone, resulted in increased expression of an ~120-kDa complex, corresponding to dimeric PKM2 (Fig. 1*G* and Fig. S3). The present study demonstrated that PKM2 nuclear translocation was stimulated in the EMT condition, suggesting a unique function of PKM2 in the nucleus.

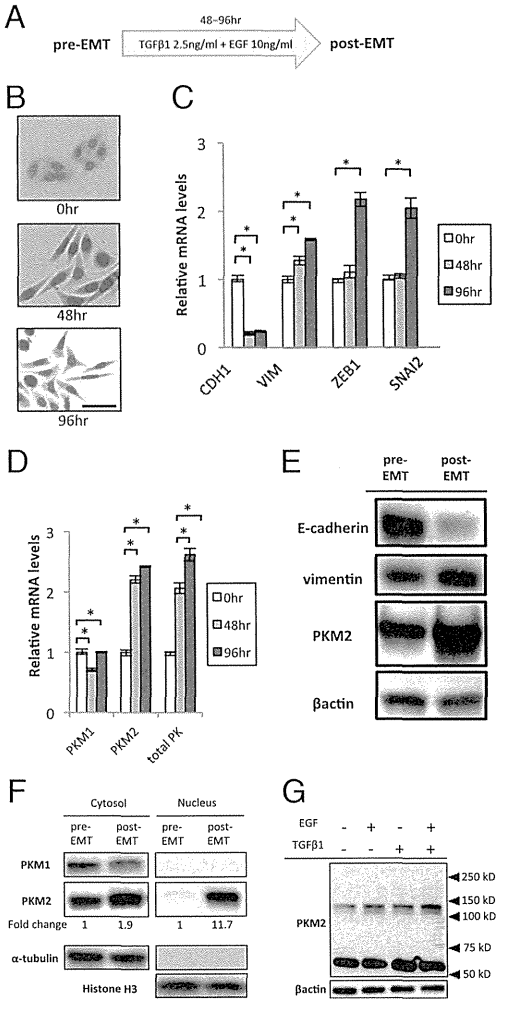

Fig. 1. PKM2 translocates into the nucleus during EMT. (*A*) Schematic representation of the procedure for EMT induction. The cells incubated for 48 h after seeding are defined as pre-EMT, and the cells cultured with 2.5 ng/mL TGF-β1 and 10 ng/mL EGF are defined as post-EMT. (*B*) Photomicrographs of the morphological change in SW480 cells. The cells were stained using the Diff-Quik Kit (Sysmex Corp.). The number of hours indicates the period since EMT induction was initiated. (Scale bar, 100 μm.) (*C*) Relative transcript (mRNA) levels of *CDH1*, *VIM*, *ZEB1*, and *SNAI2* after induction of EMT for 0, 48, and 96 h. The values at 0 h (pre-EMT) have been normalized to 1, and the data are expressed as fold. (*D*) Relative mRNA levels of PKM1, PKM2, and pyruvate kinase (total PK) after induction of EMT for 0, 48, and 96 h. (*E*) Western blot assays of E-cadherin, vimentin, and PKM2 expression in pre-EMT and post-EMT cells. Post-EMT cells were harvested at 72 h. (*F*) Western blot assays of PKM1, PKM2, α-tubulin, and histone H3 in nuclear and cytoplasmic lysates prepared from SW480 cells. With normalization to cytoplasmic tubulin or nuclear histone H3 blots, the relative intensities of PKM2 blots are shown in comparison with those in the pre-EMT condition. (*G*) SW480 cells were treated with dimethyl suberimidate for 30–60 min, immediately followed by whole cell lysis. The monomer and dimer states of PKM2 were analyzed by Western blot assay. Columns represent the average of at least three independent experiments; error bars represent the SD of the mean from triplicate results. $*P < 0.05$.

PKM2 Expression Is Required to Induce EMT. To investigate the causative role of PKM2 in EMT induction, we cultured cells with endogenous PKM2 inhibition by small interfering RNA (siRNA) knockdown (KD) under EMT conditions. We used the siRNA targeting system, which reportedly inhibits PKM2 without any off-target effects on other genes (16), and the results indicate that the most effective siRNA sequence could inhibit transcriptional and translational levels of PKM2, whereas those of PKM1 were increased (Fig. S4 *A* and *B*). PKM2 KD failed to induce spindle-shaped morphological changes under EMT conditions (Fig. 2*A*). Expression analysis indicated that PKM2 KD prevented *CDH1* down-regulation, although *VIM* expression persisted (Fig. 2*B*), suggesting a role for PKM2 in *CDH1* transcription. Fifty percent reductions in glucose or glutamine in the medium did not have significant effects on EMT marker expression (Fig. S5*A*), suggesting distinct effects on EMT and metabolism.

Western blot analysis indicated that PKM2 KD hindered *CDH1* loss and *VIM* gain compared with the control (Fig. 2*C*).

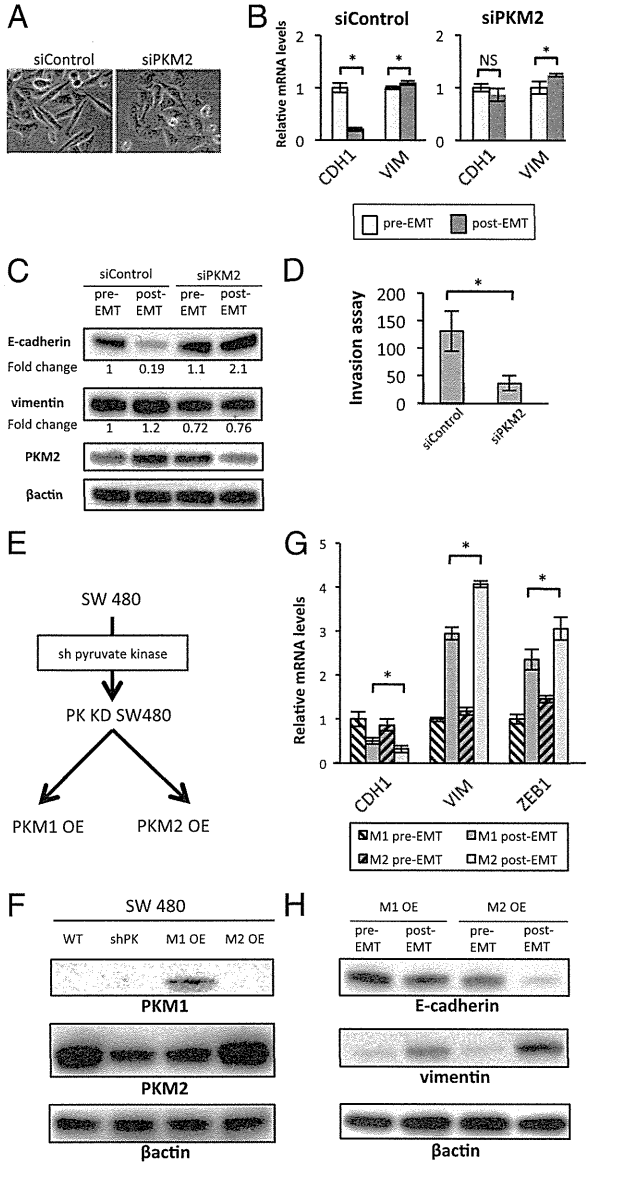

Fig. 2. PKM2 is required for EMT induction. (*A*) Phase-contrast photomicrographs of SW480 cells transfected with siControl or siPKM2 after EMT induction for 48 h. (*B*) Relative transcript (mRNA) levels of *CDH1* and *VIM* after EMT induction in cells transfected with siControl or siPKM2 for 48 h. (*C*) Western blot assays of E-cadherin, vimentin, PKM2, and β-actin expression in pre-EMT and post-EMT cells. Post-EMT cell samples were harvested at 72 h. With normalization to β-actin as a control, the relative intensities of E-cadherin and vimentin are shown in comparison with those in the control pre-EMT condition. Note that siPKM2 knockdown works efficiently in post-EMT cells. (*D*) Invasive behavior of SW480 cells treated with siControl or siPKM2. (*E*) Schematic procedure for establishing PKM1 OE or PKM2 OE SW480 cells. (*F*) Western blot assays of PKM1, PKM2, and β-actin expression in WT SW480 cells, cells stably expressing shRNA constructs targeting pyruvate kinase (shPK), and shPK cells overexpressing either PKM1 or PKM2 constructs. (*G*) Relative mRNA levels of *CDH1*, *VIM*, and *ZEB1* after EMT induction in PKM1 OE or PKM2 OE SW480 cells for 72 h. (*H*) Western blot assays of E-cadherin, vimentin, and β-actin expression in PKM1 OE and PKM2 OE cells. Post-EMT cell samples were harvested at 72 h. Column values = average of at least three independent experiments; error bars represent SD from the mean of triplicate experiments. $*P < 0.05$.

Inhibition of EMT by PKM2 KD resulted in a significant reduction in in vitro cellular invasiveness (Fig. 2*D*). The assessment of mothers against decapentaplegic homolog 2 (SMAD2) and ERK, which are downstream effectors of TGF-β1 and EGF signaling, indicated that PKM2 KD disturbed the phosphorylation process (Fig. S5*B*).

To minimize the effect of an alternative exon and to focus on the function of PKM2 in the nucleus, we established PKM1- and PKM2-overexpressing (OE) cell lines (PKM1 and PKM2 OE in Fig. 2*E*). In brief, we transfected the cells with a small hairpin RNA (shRNA) vector targeting the common region in *PK* and then introduced an overexpression vector of PKM1 or PKM2 cDNA without a complementary sequence to the shRNA (Fig. 2*F*). We cultured the established cells in EMT-inducing conditions. The results demonstrated a greater decrease in *CDH1* expression and greater increase in *VIM* and *ZEB1* expression in PKM2 OE cells compared with that in PKM1 OE cells (Fig. 2*G* and Fig. S4*C*). Consistent results were obtained by Western blot analysis (Fig. 2*H*). These results indicate that PKM2 expression is necessary for EMT induction.

Nuclear PKM2 Binds to TGIF2 and Represses CHD1 Expression. Nuclear PKM2 reportedly binds to and phosphorylates STAT3 through its function as a protein kinase (15). The observation that nuclear PKM2 increased during EMT led us to consider the possibility that PKM2 may interact with other transcription factors. To validate this hypothesis, fractions pulled-down with the PKM2 antibody were subjected to LC-electrospray ionized TOF MS analyses. The result showed that nuclear PKM2 was coimmunoprecipitated with TGIF2 and that this binding was detectable when both EGF and TGFβ1 were added to the culture (Fig. 3*A*). These findings were confirmed by immunoprecipitation, followed by Western blot analysis (Fig. 3*B*). The EMT stimulation resulted in the significant increase of TGIF2 expression (Fig. S6*A*). TGIF2 KD did not show significant alterations of PKM2 expression regardless of EMT induction (Fig. 3*E* and Fig. S6*B*). We could not detect an association of PKM1 with TGIF2 in the nucleus (Fig. S7*A*), which further supports the cytoplasmic localization of PKM1 (Fig. 1*F*).

Melhuish et al. (17) revealed that TGIF2 is a transcriptional repressor that suppresses TGF-β–responsive gene expression by binding to TGF-β–activated SMADs. First, we performed TGIF2 KD, followed by EMT induction (Fig. 3*C* and Fig. S6*B*). TGIF2 KD enhanced the decrease in both the transcriptional and the translational levels of *CDH1* expression (Fig. 3 *D* and *E*). To analyze the difference in the effect of TGIF2 KD in cells expressing either PKM1 or PKM2, we performed TGIF2 KD on PKM1 OE and PKM2 OE cells, followed by EMT induction. Interestingly, the decrease in *CDH1* expression and increase in *VIM* expression were similar at the transcriptional and translational levels after EMT induction in both cell lines (Fig. 3 *F* and *G*). These results indicate that the augmented sensitivity to EMT induction in PKM2 OE cells is abrogated under TGIF2 suppression. These data further suggest that nuclear PKM2 responds to EMT stimulation and interacts with TGIF2 to mediate EMT induction downstream of PKM2.

PKM2 and TGIF2 Recruit HDAC3 to the *CDH1* Promoter to Repress Transcription. TGIF2 is a transcriptional factor that regulates TGF-β signal transduction (17). Based on the above findings, we hypothesized that TGIF2 could bind to the *CDH1* promoter and activate *CDH1* expression in the epithelial state. To examine this hypothesis, we performed a ChIP quantitative PCR (qPCR) assay using two sets of primers located in the *CDH1* promoter sequence region (Fig. 4*A*). We found depressed binding of TGIF2 to the *CDH1* promoter region during EMT (Fig. 4*B*).

TGIF2 can control transcription by recruiting HDAC in response to TGF-β signaling (17) and PKM2 can associate with HDAC3 in the nucleus (7). To investigate whether TGIF2 can bind to HDAC3 during EMT, we performed immunoprecipitation followed by Western blot analysis and found an association between TGIF2 and HDAC3 under EMT induction (Fig. 4*C* and

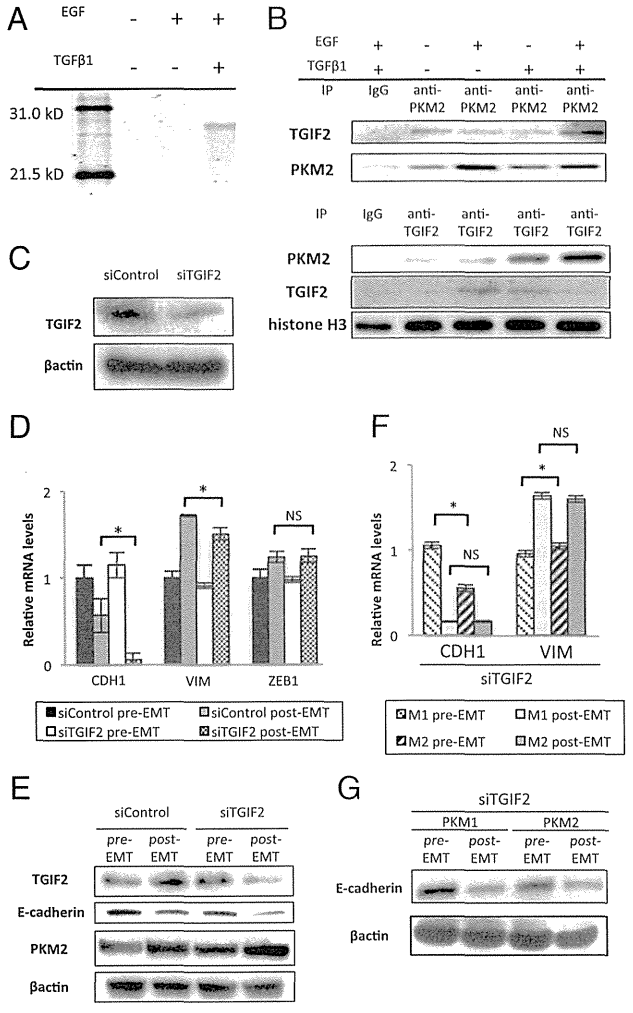

Fig. 3. Interaction between nuclear PKM2 and TGIF2 mediates EMT induction. (*A*) Polyacrylamide gel electrophoresis of proteins immunoprecipitated with anti-PKM2 antibody in the nucleic lysate of cells cultured under normal conditions, with EGF alone, or with TGF-β1 and EGF. The band detected in samples of cells stimulated with TGF-β1 and EGF was excised and analyzed by MS. (*B*) Western blot assays of immunoprecipitated samples of nucleic lysates with anti-PKM2 or anti-TGIF2 antibody. Samples were harvested after the cells were treated as indicated for 72 h. (*C*) Western blot assays of TGIF2 and β-actin expression in cells transfected with siControl or siTGIF2. (*D*) Relative transcript (mRNA) levels of *CDH1*, *VIM*, and *ZEB1* after induction of EMT in cells transfected with siControl or siTGIF2 for 72 h. (*E*) Western blot analysis of TGIF2, E-cadherin, PKM2, and β-actin expression in pre-EMT and post-EMT cells transfected with siControl or siTGIF2. Post-EMT samples were harvested at 72 h, when siRNA inhibition was profound. (*F*) Relative mRNA levels of *CDH1* and *VIM* after EMT induction in PKM1 OE and PKM2 OE cells. Post-EMT samples were harvested at 72 h. (*G*) Western blot analysis of E-cadherin and β-actin after EMT induction in PKM1 OE and PKM2 OE cells transfected with siTGIF2. Post-EMT samples were harvested at 72 h. Column values = average of at least three independent experiments; error bars represent SD from the mean of triplicate experiments. $*P < 0.05$.

Figs. S7*B* and S8). To examine the acetylation status of histone H3 in the *CDH1* promoter region, we performed ChIP qPCR and found that binding of acetylated H3K9 to the *CDH1* promoter was decreased under EMT conditions (Fig. 4*D*). Furthermore, to understand how the PKM2–TGIF2–HDAC3 complex can bind to the *CDH1* promoter, additional ChIP qPCR analysis was performed. The data indicated that similar to the binding of TGIF2, the binding of PKM2 and HDAC3 to the *CDH1* promoter was reduced during EMT (Fig. S9 *A* and *B*). Given that the TGIF2 protein bound to PKM2 and HDAC3 during EMT (Figs. 3*B* and 4*C* and Fig. S7*B*), the present study demonstrates that nuclear PKM2 plays a role in the TGIF2-dependent control of CHD1 expression and that EGF induces formation of the PKM2–TGIF2–HDAC3 complex, followed by histone deacetylation, thus resulting in suppressed *CDH1* expression. TGF-β1 may modulate the association of this complex, although H3K9 was deacetylated (Fig. 5*D*).

PKM2 Expression in the Deepest Tumor Regions Correlated with CRC Metastasis. To investigate the clinical significance of PKM2 expression in cancer metastasis, we immunohistochemically analyzed clinical CRC samples. Staining was assessed in the deepest tumor regions where the CRC invasion begins (18, 19). The

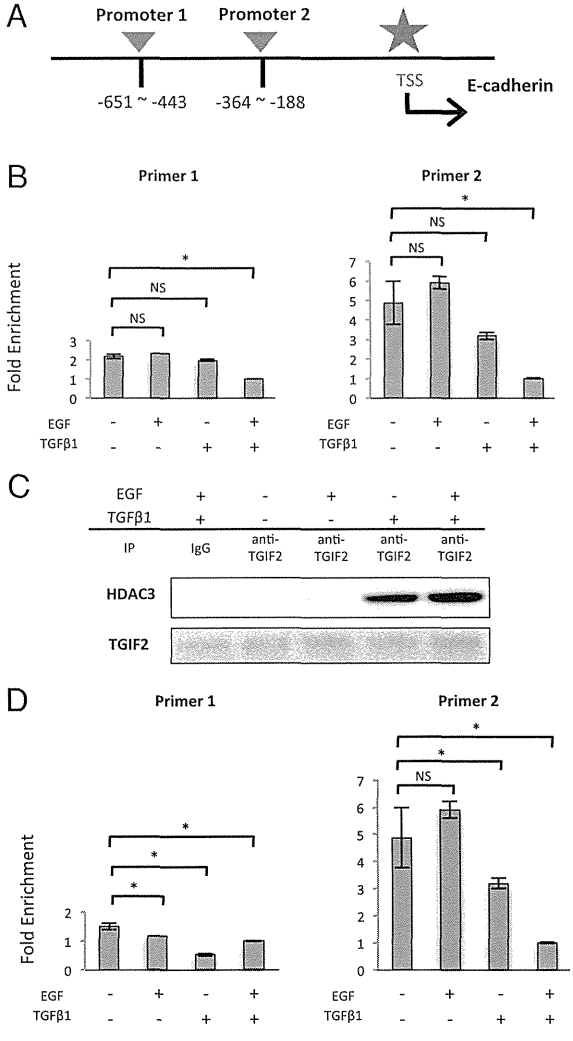

Fig. 4. TGIF2 binds to the CDH promoter and recruits HDAC3 during EMT. (*A*) Schematic diagram showing the positions of two sets of primers designed to cover the promoter region of the *CDH1* gene. (*B*) ChIP assays were performed with IgG and anti-TGIF2 antibody, followed by qPCR (mean ± SD, $n = 3$). ChIP samples were harvested from the nucleic lysate of SW480 cells treated as indicated for 72 h. (*C*) Western blot assays of immunoprecipitated samples of nucleic lysate with anti-TGIF2 antibody. Each sample was harvested after the cells were treated as indicated for 72 h. (*D*) ChIP assays were performed with IgG and anti-acetylated H3K9 antibody, followed by qPCR (mean ± SD, $n = 3$). ChIP samples were harvested from the nucleic lysate of SW480 cells treated as indicated for 72 h. Column values = average of at least three independent experiments; error bars represent SD from the mean of triplicate experiments. $*P < 0.05$.

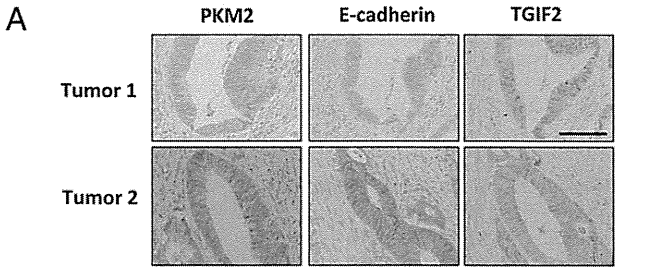

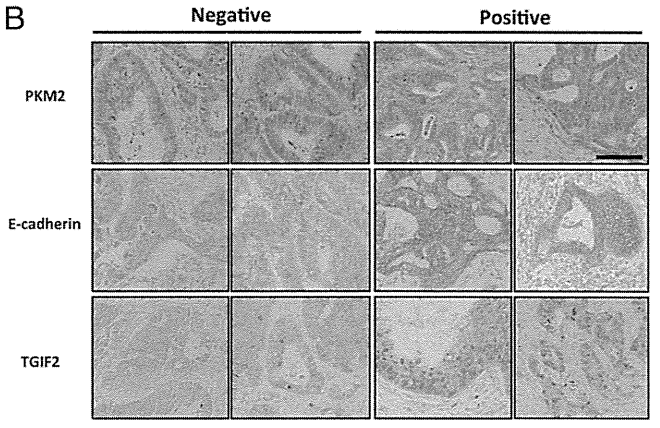

C

		PKM2 positive	PKM2 negative	P value
E-cadherin	positive	4	8	0.1698
	negative	6	2	
TGIF2	positive	10	5	0.0325
	negative	0	5	

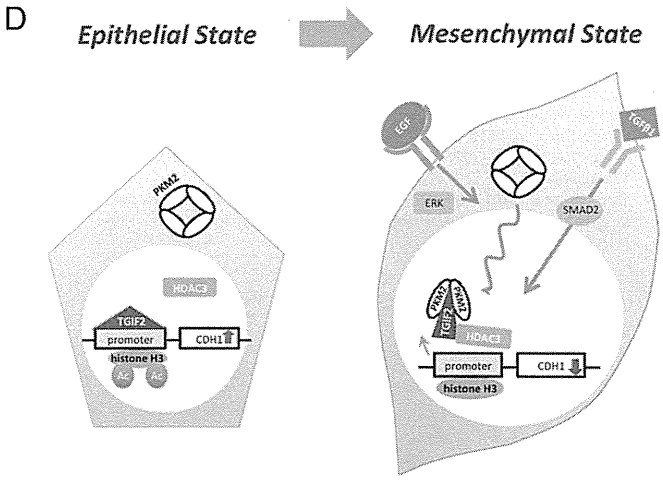

Fig. 5. The immunohistochemistry. (*A*) Staining at the invasive front, showing an inverse correlation between PKM2, E-cadherin, and TGIF2 expression. (Scale bar, 100 μm.) (*B*) The representative cases are shown for staining for PKM2, TGIF2, and E-cadherin. Invasive fronts of tumors were stained by anti-PKM2, anti-E-cadherin, and anti-TGIF2 antibodies, and the intensities were assigned to positive and negative groups. With regard to TGIF2 staining, under the microscopic observation, cases with more than 50% of cells stained in nucleus were designated as positive, whereas the others were negative. (*C*) The 10 positive and 10 negative cases for cellular PKM2 were examined for nuclear TGIF2 and membranous E-cadherin. (*D*) Theoretical model illustrating the functional roles of PKM2 and TGIF2 in regulating *CDH1* transcription during EMT.

PKM2 staining intensities were assigned to positive and negative groups (Fig. 5 *A*–*C*). The correlations between PKM2 expression and clinicopathological factors are summarized in Table S1. PKM2-positive staining was significantly correlated with metastasis to lymph nodes and distant organs. To further understand the clinical significance of PKM2 in CRC, we analyzed the GSE17536 database of the gene expression array and patient prognosis. To study the specific effect of PKM2 in the array database, we analyzed expression of both PK and its splicing factor hnRNPA2, because hnRNPA2 stimulates the splicing to PKM2 (20, 21). As expected, cases with high PK and high hnRNPA2 expression showed a poorer prognosis than other groups; the difference in prognosis was apparent in stages III and IV with metastasis (Fig. S10 *A* and *B*). The data confirmed that PKM2 can enhance the ability of cancer cells to metastasize in primary cancer tissues.

Discussion

In the present study, we demonstrated that nuclear PKM2 interacts with TGIF2 during EMT, which is pivotal in promoting the transition into the mesenchymal cancer cell phenotype. Consequently, we propose a model for the nuclear PKM2 function in response to EMT stimulation (Fig. 5*D*). Under epithelial conditions, histone H3 is acetylated on the *CDH1* promoter region and *CDH1* is transcribed where TGIF2 should serve as an active transcription factor. Once the EMT signal stimulates transformation of the cancer cell, a PKM2 fraction enters the nucleus and associates with TGIF2. We assume that this association will alter the conformation of TGIF2 or its associated complexes, effectively loosening the binding between TGIF2 and the *CDH1* promoter sequence to allow the recruitment of HDAC3 and subsequent histone H3 deacetylation. *CDH1* expression is suppressed as a consequence of the downregulated promoter activity. In this context, nuclear PKM2 serves as a transcriptional cofactor regulating TGIF2 behavior.

Few reports have investigated the significance of TGIF2 in cancer. In ovarian cancer, TGIF2 is reportedly amplified and overexpressed (22), whereas a comparison between colorectal adenoma and colorectal carcinoma revealed that TGIF2 expression is increased only in the latter (23). Further, TGIF2 has been shown to interact with TGF-β–activated SMADs and be able to repress the activation of TGF-β–responsive transcription (17). The present study demonstrated that TGIF2 affects *CDH1* expression through the regulation of promoter activity in which TGIF2 is supposed to function as an activating transcription factor.

TGF-β1 is a multifunctional cytokine that has dual and opposing roles in controlling cell fate. In the early stages of cancer, TGF-β1 induces growth arrest and apoptosis, exerting tumor-suppressive effects, whereas in later stages, TGF-β1 enhances tumor progression by provoking a variety of malignancy-related responses, including EMT (24–26). This paradox remains unsolved despite numerous studies addressing the issue. However, based on the results in the present study, we propose that the interaction between PKM2 and TGIF2 may offer a plausible explanation. In normal cells, PK expression is exclusively shifted to PKM1, but on TGF-β signaling, TGIF2 can suppress transcription downstream of the SMAD signal. Conversely, in cancer cells abundantly expressing PKM2, PKM2 translocates and is bound to TGIF2 in the nucleus, thereby reversing TGF-β signal transduction. Further investigation is necessary to determine the significance of TGIF2 expression and the precise mechanism underlying this interaction.

Nuclear PKM2 forms a dimer and functions as a protein kinase, whereas cytoplasmic PKM2 forms a tetramer and functions as a pyruvate kinase (15). In the present study, the dimeric form of PKM2 was increased, suggesting that the protein kinase activity of PKM2 is enhanced during EMT. PKM2 translocates into the nucleus in response to variable signals, of which, the EGF–ERK pathway is the most investigated (7, 27). Interestingly, TGIF2 is phosphorylated in response to EGF signaling (17). Given that EGF induces nuclear translocation of PKM2, PKM2 may function as a dimeric protein kinase in the

nucleus, phosphorylating TGIF2. However, the phosphorylation status of TGIF2 was not addressed in our study. Gao et al. (15) demonstrated that PKM2 interacts with STAT3 to control downstream gene expression in SW480 cells. Thus, it is conceivable that the molecular interaction of PKM2 is highly context dependent, with cell fate determined by how nuclear PKM2 regulates gene expression.

PKM2 has both metabolic and nonmetabolic functions, which are essential in the cytoplasm and nucleus, respectively. Increasing evidence has suggested that nuclear PKM2 binds to numerous transcriptional factors, thereby conferring cells with advanced malignant potential. The present study determined that PKM2 significantly influences EMT induction by modulating *CDH1* expression, thus providing a molecular basis for EMT acquisition. Future cancer treatments may be able to target the inhibition of nuclear PKM2.

Methods

Cell Lines and Culture. The human colorectal cancer cell lines, SW480 and HCT116, were obtained from ATCC, and CaR-1 was obtained from JCRB. These cell lines were grown in DMEM (Sigma-Aldrich) supplemented with 10% (vol/vol) FBS (Thermo Fisher Scientific), 100 U/mL penicillin, and 100 U/mL streptomycin (Life Technologies) and grown at 37 °C in a humidified incubator with 5% CO_2.

EMT Induction. Cells were seeded at a concentration of 5.0×10^4 cells/mL and incubated in a humidified atmosphere (37 °C and 5% CO_2) in standard medium for 48 h, after which they were treated with TGF-β1 (2.5 ng/mL; Sigma-Aldrich). Next, they were incubated with MEM supplemented with 10 ng/mL FBS-free EGF (Sigma-Aldrich), 100× insulin-transferring selenium (ITS; Life Technologies), and 50 nmol/L hydrocortisone (Tokyo Kasei) for 48–96 h.

ACKNOWLEDGMENTS. We thank the members of our laboratories for helpful discussions; Idea Consultants, Inc. (Osaka, Japan) and Olympus Co. (Tokyo, Japan) for technical assistance; Lewis C. Cantley for providing the lentiviral shRNA and retroviral expression vector; and H. Miyoshi for providing the packaging plasmids.

1. Jemal A, et al. (2011) Global cancer statistics. *CA Cancer J Clin* 61(2):69–90.
2. Warburg O (1956) On the origin of cancer cells. *Science* 123(3191):309–314.
3. Vander Heiden MG, Cantley LC, Thompson CB (2009) Understanding the Warburg effect: The metabolic requirements of cell proliferation. *Science* 324(5930):1029–1033.
4. Christofk HR, et al. (2008) The M2 splice isoform of pyruvate kinase is important for cancer metabolism and tumour growth. *Nature* 452(7184):230–233.
5. Hacker HJ, Steinberg P, Bannasch P (1998) Pyruvate kinase isoenzyme shift from L-type to M2-type is a late event in hepatocarcinogenesis induced in rats by a choline-deficient/DL-ethionine-supplemented diet. *Carcinogenesis* 19(1):99–107.
6. Elbers JR, et al. (1991) Pyruvate kinase activity and isozyme composition in normal fibrous tissue and fibroblastic proliferations. *Cancer* 67(10):2552–2559.
7. Yang W, et al. (2011) Nuclear PKM2 regulates β-catenin transactivation upon EGFR activation. *Nature* 480(7375):118–122.
8. Luo W, et al. (2011) Pyruvate kinase M2 is a PHD3-stimulated coactivator for hypoxia-inducible factor 1. *Cell* 145(5):732–744.
9. Hanahan D, Weinberg RA (2011) Hallmarks of cancer: The next generation. *Cell* 144(5):646–674.
10. Weinberg RA (2008) Mechanisms of malignant progression. *Carcinogenesis* 29(6): 1092–1095.
11. Rees JR, Onwuegbusi BA, Save VE, Alderson D, Fitzgerald RC (2006) In vivo and in vitro evidence for transforming growth factor-beta1-mediated epithelial to mesenchymal transition in esophageal adenocarcinoma. *Cancer Res* 66(19):9583–9590.
12. Yokobori T, et al. (2013) Plastin3 is a novel marker for circulating tumor cells undergoing the epithelial-mesenchymal transition and is associated with colorectal cancer prognosis. *Cancer Res* 73(7):2059–2069.
13. Okada H, Danoff TM, Kalluri R, Neilson EG (1997) Early role of Fsp1 in epithelial-mesenchymal transformation. *Am J Physiol* 273(4 Pt 2):F563–F574.
14. Strutz F, et al. (2002) Role of basic fibroblast growth factor-2 in epithelial-mesenchymal transformation. *Kidney Int* 61(5):1714–1728.
15. Gao X, Wang H, Yang JJ, Liu X, Liu ZR (2012) Pyruvate kinase M2 regulates gene transcription by acting as a protein kinase. *Mol Cell* 45(5):598–609.
16. Goldberg MS, Sharp PA (2012) Pyruvate kinase M2-specific siRNA induces apoptosis and tumor regression. *J Exp Med* 209(2):217–224.
17. Melhuish TA, Gallo CM, Wotton D (2001) TGIF2 interacts with histone deacetylase 1 and represses transcription. *J Biol Chem* 276(34):32109–32114.
18. Lugli A, Karamitopoulou E, Zlobec I (2012) Tumour budding: A promising parameter in colorectal cancer. *Br J Cancer* 106(11):1713–1717.
19. Ueno H, et al. (2014) Novel risk factors for lymph node metastasis in early invasive colorectal cancer: A multi-institution pathology review. *J Gastroenterol* 49(9):1314–1323.
20. Clower CV, et al. (2010) The alternative splicing repressors hnRNP A1/A2 and PTB influence pyruvate kinase isoform expression and cell metabolism. *Proc Natl Acad Sci USA* 107(5):1894–1899.
21. David CJ, Chen M, Assanah M, Canoll P, Manley JL (2010) HnRNP proteins controlled by c-Myc deregulate pyruvate kinase mRNA splicing in cancer. *Nature* 463(7279): 364–368.
22. Imoto I, et al. (2000) Amplification and overexpression of TGIF2, a novel homeobox gene of the TALE superclass, in ovarian cancer cell lines. *Biochem Biophys Res Commun* 276(1):264–270.
23. Lips EH, et al. (2008) Integrating chromosomal aberrations and gene expression profiles to dissect rectal tumorigenesis. *BMC Cancer* 8:314.
24. Roberts AB, Wakefield LM (2003) The two faces of transforming growth factor beta in carcinogenesis. *Proc Natl Acad Sci USA* 100(15):8621–8623.
25. Tian M, Schiemann WP (2009) The TGF-beta paradox in human cancer: An update. *Future Oncol* 5(2):259–271.
26. Rahimi RA, Leof EB (2007) TGF-beta signaling: A tale of two responses. *J Cell Biochem* 102(3):593–608.
27. Yang W, et al. (2012) ERK1/2-dependent phosphorylation and nuclear translocation of PKM2 promotes the Warburg effect. *Nat Cell Biol* 14(12):1295–1304.

Cancer Science
Japanese Cancer Association JCA
Open Access

Combined evaluation of hexokinase 2 and phosphorylated pyruvate dehydrogenase-E1α in invasive front lesions of colorectal tumors predicts cancer metabolism and patient prognosis

Atsushi Hamabe,[1] Hirofumi Yamamoto,[1] Masamitsu Konno,[2] Mamoru Uemura,[1] Junichi Nishimura,[1] Taishi Hata,[1] Ichiro Takemasa,[1] Tsunekazu Mizushima,[1] Naohiro Nishida,[2] Koichi Kawamoto,[1] Jun Koseki,[3] Yuichiro Doki,[1] Masaki Mori[1] and Hideshi Ishii[2,3,4]

Departments of [1]Gastroenterological Surgery; [2]Frontier Science for Cancer and Chemotherapy; [3]Cancer Profiling Discovery, Graduate School of Medicine, Osaka University, Osaka, Japan

Key words

Colorectal cancer, hexokinase, invasion, metastasis, pyruvate dehydrogenase

Correspondence

Hideshi Ishii, Department of Frontier Science for Cancer and Chemotherapy, Graduate School of Medicine, Osaka University, Suita, Yamadaoka 2-2, Osaka 565-0871, Japan. Tel: +81-(0)6-6879-2641, 2640; Fax: +81-(0)6-6879-2639; E-mail: hishii@gesurg.med.osaka-u.ac.jp

Funding information

Ministry of Education, Culture, Sports, Science, and Technology Third Comprehensive 10-year Strategy for Cancer Control, Ministry of Health, Labor, and Welfare Kobayashi Cancer Research Foundation Princess Takamatsu Cancer Research Fund, Japan National Institute of Biomedical Innovation Osaka University Drug Discovery Funds.

Received March 10, 2014; Revised June 22, 2014; Accepted July 4, 2014

Cancer Sci **105** (2014) 1100–1108

doi: 10.1111/cas.12487

Although numerous studies have shown the significance of cancer-specific aerobic glycolysis, how glycolysis contributes to tumor invasion, a critical phenomenon in metastasis, remains unclear. With regard to colorectal cancer (CRC), we studied two critical gate enzymes, hexokinase 2 (HK2), which is involved in glycolysis, and phosphorylated pyruvate dehydrogenase-E1α (p-PDH), which is involved in oxidative phosphorylation (OxPhos). Immunohistochemical analyses using anti-HK2 and p-PDH antibodies were performed on surgically resected CRC samples (n = 104), and the expression in invasive front lesions of tumors was assessed. Positive HK2 expression correlated with extensive tumor diameter (P = 0.0460), advanced tumor depth (P = 0.0395), and presence of lymph node metastasis (P = 0.0409). Expression of p-PDH tended to be higher in right-sided CRCs than in left-sided CRCs (P = 0.0883). In survival analysis, the combined evaluation of positive HK2 and negative p-PDH was associated with reduced recurrence-free survival (RFS) (P = 0.0169 in all stages and P = 0.0238 in Stage II and III patients, respectively). This evaluation could predict RFS more precisely than the independent evaluation. The present study indicated that high HK2 expression combined with low p-PDH expression in the invasive front lesions of CRC tumors is predictive of tumor aggressiveness and survival of CRC cases.

Colorectal cancer (CRC) is the second most common cancer in the world. Each year, >1.2 million individuals develop CRC, and approximately 600 000 deaths occur.[1] Although the efficacy of treatment has been gradually improving because of advances in chemotherapy or surgical technologies, the prognosis of patients with distant metastases and recurrence has not improved much. Numerous studies have shown that the activation of tumor-promoting genes and inactivation of growth-constraint tumor suppressor genes through genetic and epigenetic alterations contribute to the activation of biological phenomena, such as cell invasion, movement, and colonization, in distant organs during the metastatic process[2,3]; however, the precise molecular mechanisms involving biologically active metabolites in cancer are not completely understood.

Recent studies have indicated that deregulation in intratumor metabolism is involved in malignant behaviors of cancer cells.[4,5] In glucose metabolism, lactate is preferentially produced in cancer cells, even in the presence of adequate oxygen in culture, a critical biological phenomenon termed aerobic glycolysis or the Warburg effect.[6] Pyruvate kinase M2 (PKM2) was identified as a key molecule involved in the Warburg effect.[7] Subsequently, at least three other enzymes, including phosphofructokinase 1, hexokinase 2 (HK2), and a phosphorylated form of pyruvate dehydrogenase-E1α (p-PDH), have been shown to be involved in cancer-associated metabolism, including glycolysis and oxidative phosphorylation (OxPhos) in the mitochondria.[8–10] Aerobic glycolysis is thought to be beneficial for the production of biomass, such as nucleic acids and lipids, and reduced forms of glutathione, thereby conferring the advantages of low oxidative stress and selective growth.

In the initial step of glycolysis, HK converts glucose and ATP to glucose-6-phosphate and ADP. Four HK isoforms, HK1, HK2, HK3, and HK4, which are encoded by separate genes,[11] are expressed in mammals. In adult tissues, HK1 is

© 2014 The Authors. Cancer Science published by Wiley Publishing Asia Pty Ltd on behalf of Japanese Cancer Association.
This is an open access article under the terms of the Creative Commons Attribution-NonCommercial-NoDerivs License, which permits use and distribution in any medium, provided the original work is properly cited, the use is non-commercial and no modifications or adaptations are made.

ubiquitously expressed, whereas HK2 is expressed in limited types of tissues, such as adipose tissues, skeletal muscles, and the heart.[12] In cancer cells, HK2 and, to a lesser extent, HK1 are expressed,[13] which suggests a preferential role of HK2 in the glucose flux of cancer cells. Recent studies have indicated that HK2 is necessary for the tumorigenicity of non-small cell lung cancer and breast cancer in humans, whereas HK2 deletion results in rapid suppression of tumor growth.[9]

Pyruvate dehydrogenase has a gate-keeper role in a branching point that links glycolysis to OxPhos in the citric acid cycle by converting pyruvate to acetyl-CoA in the mitochondria. The catalyzing activity of PDH is inhibited by phosphorylation at serine residue(s) by PDH kinase (PDK), whereas PDH is activated by PDH phosphatase.[14,15] Reportedly, the process of aerobic glycolysis is at least partially maintained by the attenuation of mitochondrial function through PDH inhibition.[16] A melanoma study showed that PDH inactivation by serine 293-phosphorylation by PDK led to high tumorigenic activity, whereas PDK depletion resulted in hypophosphorylation of PDH, regression of tumors, and further eradication of subpopulations resistant to a specific inhibitor to oncogene $BRAF^{V600E}$,[17] which suggested an exclusive dependency on aerobic glycolysis of melanoma growth.

In the present study, we immunohistochemically analyzed the expression of HK2 and p-PDH in the invasive front lesions of clinical CRC samples and assessed their ability to predict tumor aggressiveness and survival. We identified an unexpected association of p-PDH with improved survival and showed that combined expression of HK2 and p-PDH was predictive of patient survival. Furthermore, we induced epithelial–mesenchymal transition (EMT) to colon cancer cell, followed by biochemical assays of HK and PDH. These results suggest a unique role of p-PDH in CRC growth at invasive fronts.

Materials and Methods

Clinical tissue samples. Colorectal tissue samples (n = 104) were collected during surgery (2007–2009) at the Department of Surgery, Osaka University. None of the patients had undergone preoperative chemotherapy or irradiation. Samples were fixed in buffered formalin at 4°C overnight, processed through graded ethanol solutions, and embedded in paraffin. The specimens were appropriately used under the approval of the ethics committee at the Graduate School of Medicine, Osaka University.

Immunohistochemistry. Tissue sections (3.5 μm thick) were prepared from paraffin-embedded blocks. After antigen retrieval treatment in 10 mM citrate buffer (pH 6.0) at 115°C for 15 min using Decloaking Chamber NxGen (Biocare Medical, Concord, CA, USA), immunostaining was performed using the Vectastain ABC Peroxidase Kit (Vector Laboratories, Burlingame, CA, USA). Antibodies used for immunohistochemistry were anti-HK2 rabbit antibody (2867; Cell Signaling Technology, Danvers, MA, USA), anti-pyruvate dehydrogenase E1α subunit (PDH-E1α) mouse antibody (ab110330; Abcam, Cambridge, UK), and pSer293 (p-PDH), the anti-phosphorylated form of PDH-E1α rabbit antibody (AP1062; Millipore, Darmstadt, Germany). The specificity of the antibodies was confirmed by the data showing that each antibody detected single band corresponding to the targeted protein in Western blot analysis (Suppl. Figs S1–3), and additionally, in regard to HK2 antibody, the absorption test was carried out in immunohistochemical analysis (Suppl. Fig. S4). The slides were incubated overnight at 4°C at the following dilutions: anti-HK2 antibody, 1:200; anti-p-PDH, 1:500; anti-PDH-E1α, 1:200. Sections were counterstained with hematoxylin. We rated the intensity of staining on a scale of 0 to 2: 0, negative; 1, weak; and 2, strong. We used pancreatic tissue as a positive control of HK2 according to the previous study,[18] and a case of Stage I rectal cancer, the staining of which at the deepest part was strong as a positive control of p-PDH. Phosphate buffered saline instead of the antibodies was used as a negative control. We assigned colorectal tissue stained as intense as the positive control to "intensity score 2", while unstained colorectal tissue similar to the negative control was assigned to "score 0" (Fig. 1). The tissue stained weaker than the positive control but stronger than the negative control was categorized into "score 1" (Fig. 1b,c). The intensity at the deepest part of the tumor was recorded in each sample. The reason why the intensity at the deepest part of the tumor was assessed was that the cancer cell was stimulated to invade into surrounding tissues at this region.[19,20]

Assessment of tumor budding. Tumor budding was estimated according to the definition proposed by Ueno *et al.*[21,22] An isolated cancer cell or a cluster composed of fewer than five cancer cells was defined as tumor budding. The number of buddings was counted in the field under a magnification of ×200 in the invasive front area.

Cell lines and culture. Human colon cancer cell line, SW480, was obtained from the ATCC (Manassas, VA, USA). The cells were grown in Dulbecco's modified Eagle's medium (DMEM) supplemented with 10% FBS, 100 U/mL penicillin, and 100 U/mL streptomycin, and grown at 37°C in a humidified incubator with 5% CO_2.

Induction of EMT. Cells were seeded at the concentration of 5.0×10^4 cells/mL and incubated in a humidified atmosphere (37°C and 5% CO_2) in standard medium for 48 h. After 48 h incubation, the cells were treated with transforming growth factor-β1 (TGF-β1) (2.5 ng/mL) and were incubated with MEM medium supplemented with FBS free, 10 ng/mL epidermal

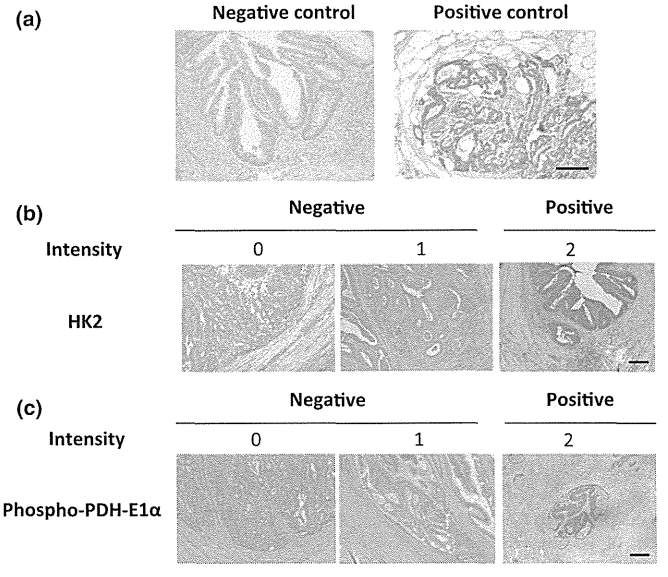

Fig. 1. Immunohistochemical analysis of HK2 and p-PDH in clinical colorectal cancer samples. (a) Phosphate buffered saline was used as a negative control and a case of pancreatic cancer tissue was used as a positive control for HK2. (b) Staining of HK2 and (c) p-PDH at the invasive front are shown; the intensity was rated in three stages. Scale bar, 200 μm.

© 2014 The Authors. Cancer Science published by Wiley Publishing Asia Pty Ltd on behalf of Japanese Cancer Association.

growth factor (Sigma-Aldrich, St Louis, MO, USA), 100 × insulin/transferring/selenium (ITS) (Life Technologies, Carlsbad, CA, USA), and 50 nmol/L hydrocortisone (Tokyo Kasei, Tokyo, Japan) for 48–72 h.

Biochemical assay. Biochemical activities of SW480 were analyzed using Hexokinase Colorimetric Assay Kit (ab136957; Abcam) for hexokinase activity and Pyruvate dehydrogenase Enzyme Activity Microplate Assay Kit (ab109902; Abcam) for pyruvate dehydrogenase activity according to the manufacturer's instructions.

Western blot analysis. Total protein was extracted from the cell lines in radio immunoprecipitation assay (RIPA) buffer (Thermo Fisher Scientific, Rockford, IL, USA). Aliquots of protein were electrophoresed on SDS-PAGE, Tris-HCl gels (Bio-Rad Laboratories, Hercules, CA, USA). The separated proteins were transferred to PVDF membranes using iBlot (Life Technologies). Antibodies specific to E-cadherin (3195; Cell Signaling Technology), Vimentin (5741; Cell Signaling Technology), ACTB (A2103, Sigma-Aldrich) were used in addition to the antibodies used for immunohistochemistry. The membranes were incubated with primary antibodies overnight at 4°C, at appropriate concentrations (1:1000 for E-cadherin; 1:1000 for Vimentin; 1:1000 for HK2; 1:1000 for PDH-E1α; 1:10 000 for p-PDH: 1:2000 for ACTB) followed by the incubation with horseradish-peroxidase-linked anti-rabbit or mouse IgG (GE Healthcare Biosciences, Piscataway, NJ, USA) at a dilution of 1:100 000 for 1 h at room temperature. The antigen–antibody complex was detected with the ECL Prime Western Blotting Detection Kit (GE Healthcare Biosciences).

Quantitative reverse transcription polymerase chain reaction. Total RNA was extracted from cultured cells using RNeasy Mini Kit and QIA shredder (Qiagen, Valencia, CA, USA). Complemetary DNA was synthesized with ReverTra Ace reverse transcriptase (Toyobo, Osaka, Japan). Real-time quantitative polymerase chain reactions (qRT-PCR) were conducted with the LightCycler-FastStart DNA Master SYBR

Table 1. HK 2 expression and clinicopathological features of colorectal cancer

Hexokinase 2	Positive (n = 61)	Negative (n = 43)	P-value
Patient background			
Gender (Male/Female)	37/24	28/15	0.6436
Age (mean ± SD)	63.2 ± 12.4	66.6 ± 10.6	0.9265
BMI (kg/m^2)	22.2 (20.5, 26.1)	22.4 (20.3, 25.2)	0.9579
CEA (ng/mL)	3 (2, 9)	3 (1, 5)	0.5232
CA19-9 (U/mL)	11 (7, 21)	13 (5, 22)	0.8013
Tumor characteristics			
Tumor diameter (mm)	40 (25, 54)	30 (20, 44)	0.0460*
Location			
C/A/T	5/10/7	3/5/7	0.9013
D/S/R	2/13/24	2/7/19	
Tumor type			
Type 0	13	13	0.3008
Type 1/2/3/4/5	3/32/12/0/1	3/22/4/0/1	
Histological type			
tub1/tub2/pap	17/39/1	13/23/1	0.3118
por/muc	0/4	4/2	
Depth			
T0/T1/T2	5/5/13	3/10/12	0.0395*
T3/T4	31/7	15/3	
Lymph node metastasis			
N0	35	33	0.0409*
N1/N2/N3	16/7/3	7/0/3	
Distant metastasis			
M0	53	40	0.5190
M1	8	3	
Lymphatic duct invasion			
ly0	15	19	0.2321
ly1/ly2	34/12	21/3	
Venous invasion			
v0	48	36	0.6176
v1/v2	9/4	7/0	
Stage			
0/I/II	5/13/15	3/20/9	0.0350*
IIIa/IIIb/IV	13/7/8	6/2/3	

*Statistically significant. Data are presented as median (first quartile, third quartile). A, ascending colon; BMI, body mass index; C, cecum; D, descending colon; muc, mucinous carcinoma; pap, papillary adenocarcinoma; por, poorly differentiated adenocarcinoma; R, rectum; S, sigmoid colon; T, transverse colon; tub1, well-differentiated adenocarcinoma; tub2, moderately differentiated adenocarcinoma.

Table 2. p-PDH expression and clinicopathological features of colorectal cancer

Phospho-PDH-E1α	Positive (n = 34)	Negative (n = 70)	P-value
Patient background			
Gender (Male/Female)	22/12	43/27	0.7461
Age (mean ± SD)	66.0 ± 10.4	63.5 ± 13.3	0.1669
BMI (kg/m^2)	23.6 (20.6, 25.6)	21.9 (20.3, 25.6)	0.4316
CEA (ng/mL)	2.5 (1, 6)	3 (2.0, 7.3)	0.4401
CA19-9 (U/mL)	12.5 (5.0, 23.3)	12.5 (7.0, 21.3)	0.8538
Tumor characteristics			
Tumor diameter (mm)	37 (22, 52)	35 (22, 52)	0.6126
Location			
C/A/T	5/6/5	3/9/9	0.0883
D/S/R	3/3/12	1/17/31	
Tumor type			
Type 0	11	15	0.2275
Type 1/2/3/4/5	1/16/4/0/2	5/38/12/0/0	
Histological type			
tub1/tub2/pap	10/18/1	20/44/1	0.2893
por/muc	2/3	2/3	
Depth			
T0/T1/T2	3/4/7	5/11/18	0.4779
T3/T4	16/4	30/6	
Lymph node metastasis			
N0	23	45	0.7354
N1/N2/N3	5/4/2	18/3/4	
Distant metastasis			
M0	29	64	0.3339
M1	5	6	
Lymphatic duct invasion			
ly0	12	22	0.6857
ly1/ly2	15/7	40/8	
Venous invasion			
v0	26	58	0.4394
v1/v2	7/1	9/3	
Stage			
0/I/II	3/9/10	5/24/14	0.7461
IIIa/IIIb/IV	4/3/5	15/6/6	

Data are presented as median (first quartile, third quartile). A, ascending colon; BMI, body mass index; C, cecum; D, descending colon; muc, mucinous carcinoma; pap, papillary adenocarcinoma; por, poorly differentiated adenocarcinoma; R, rectum; S, sigmoid colon; T, transverse colon; tub1, well-differentiated adenocarcinoma; tub2, moderately differentiated adenocarcinoma.

© 2014 The Authors. Cancer Science published by Wiley Publishing Asia Pty Ltd on behalf of Japanese Cancer Association.